

Modulation of equatorial Pacific sea surface temperature response to westerly wind events by the oceanic background state

Martin Puy¹ · Jérôme Vialard¹ · Matthieu Lengaigne^{1,2} · Eric Guilyardi^{1,3} · Aurore Voltaire⁴ · Gurvan Madec¹

Received: 28 January 2016 / Accepted: 29 November 2016 / Published online: 20 December 2016
© Springer-Verlag Berlin Heidelberg 2016

Abstract Equatorial Pacific Westerly Wind Events (WWEs) impact ENSO evolution through their local and remote oceanic response. This response depends upon the WWE properties (duration, intensity, fetch...) but also on the underlying oceanic state. Oceanic simulations with an identical idealised western Pacific WWE applied every 3 months on seasonally and interannually varying oceanic conditions over the 1980–2012 period allow characterizing and understanding the modulation of the WWE response by the oceanic background state. These simulations reveal that the amplitude of the Sea Surface Temperature (SST) response, which can vary by one order of magnitude, is far more sensitive to the oceanic background conditions than the dynamical response to WWEs. The amplitude of the surface-flux driven cooling in the western Pacific is strongly modulated by zonal advection, through interannual variations in the background SST zonal gradient. The

amplitude of the warming at the warm pool eastern edge is controlled by horizontal advection, and varies as a function of the zonal SST gradient and distance between the WWE and warm pool eastern edge. The amplitude of the eastern Pacific warming varies as a function of the background thermocline depth and local winds. Overall, only the amplitude of the WWE-driven western Pacific cooling can be clearly related to the phase of ENSO, while the WWE driven SST response in the central and eastern Pacific is more diverse and less easily related to large-scale properties. The implications of these findings for ENSO predictability are discussed.

Keywords WWE · ENSO · Wind events · Oceanic background state

1 Introduction

The El Niño Southern Oscillation (ENSO) is the dominant mode of interannual climate variability at global scale. The positive phase of ENSO is associated with anomalously warm Sea Surface Temperatures (SSTs) in the central and eastern equatorial Pacific, with planetary-scale impacts (e.g. McPhaden et al. 2006a) through atmospheric teleconnections (Trenberth et al. 1998). Because of its socio-economic consequences, modelling and forecasting ENSO is of crucial importance but remains a challenge (Barnston and Tippett 2012; Vecchi and Wittenberg 2010; Guilyardi et al. 2012; Capotondi et al. 2015). The predictability of ENSO is grounded on our current understanding of its underlying mechanisms. El Niño events develop as the result of the Bjerknes feedback (Bjerknes 1966), a positive air-sea feedback loop where the westerly wind response to a positive SST anomaly in the central Pacific drives an

This paper is a contribution to the special collection on ENSO Diversity. The special collection aims at improving understanding of the origin, evolution, and impacts of ENSO events that differ in amplitude and spatial patterns, in both observational and modeling contexts, and in the current as well as future climate scenarios. This special collection is coordinated by Antonietta Capotondi, Eric Guilyardi, Ben Kirtman and Sang-Wook Yeh

✉ Martin Puy
Martin.Puy@locean-ipsl.upmc.fr

- ¹ LOCEAN/IPSL (Sorbonne Universités, UPMC, Univ Paris 06-CNRS-IRD-MNHN), Case 100, Université P. et M. Curie, 4, Place Jussieu, 75252 Paris Cedex 05, France
- ² Indo-French Cell for Water Sciences, IISc-NIO-IITM-IRD Joint International Laboratory, NIO, Goa, India
- ³ NCAS-Climate, University of Reading, Reading, UK
- ⁴ CNRM-GAME/GMGEC/ASTER, Météo France, Toulouse, France

oceanic signal that reinforces the initial warming. This positive feedback mechanism is offset by a number of negative feedbacks, such as the dynamical feedback associated with the mean atmospheric circulation and thermodynamical feedbacks associated with air-sea fluxes (see Wang and Picaut 2004 for a review). The delayed negative feedback from oceanic dynamics is essential to provide a mechanism for ENSO termination (e.g., Schopf and Suarez 1988). In the recharge oscillator paradigm (Jin 1997), ENSO wind anomalies generate a Sverdrup response that drives upper ocean heat content away from the equatorial strip during ENSO warm phase, favouring the transition to its negative phase. The converse mechanism then allows for the recharge of the equatorial heat content and preconditions the development of a new El Niño event. ENSO predictability largely results from this ocean subsurface memory, the equatorial Pacific heat content leading ENSO SST evolution by ~8 months (e.g. Meinen and McPhaden 2000).

This ENSO predictability is, however, strongly hampered by high frequency wind variations, whose details are not predictable at long lead-times. A large body of literature indeed points towards an important role of intraseasonal wind variability in ENSO dynamics and predictability (Kleeman and Moore 1999; Zavala-Garay et al. 2005; McPhaden et al. 2006; Shi et al. 2009; Wang et al. 2011; Chen et al. 2015). A large part of this high frequency forcing occurs in the form of Westerly Wind Events (WWEs), characterized as episodes of anomalous, short-lived, but strong westerlies developing over the western Pacific warm pool (e.g., Luther and Harrison 1984; Lengaigne et al. 2004a). These WWEs promote the onset and/or development of El Niño events (Fedorov 2002; Boulanger et al. 2004; Lengaigne et al. 2004b) and contribute to the irregularity of ENSO, in terms of timing (its broad spectrum ranging between 2 and 7 years; e.g., Gebbie et al. 2007; Jin et al. 2007), magnitude (Eisenman et al. 2005; Gebbie et al. 2007) and spatial patterns (Hu et al. 2014; Lian et al. 2014; Fedorov et al. 2014).

Contrasting the tropical Pacific evolution in 2014 against that of 1997 or 2015 provides a compelling illustration of the important role of WWEs in ENSO evolution. The volume of warm water in the equatorial band was anomalously high (>1 std) in early 1997 (McPhaden 1999), 2014 (McPhaden 2015) and 2015 (TAO website <http://www.pmel.noaa.gov/tao/>), with a warm pool anomalously shifted east. Despite such similar oceanic conditions, and the occurrence of WWEs during the first 3 months of the year, these 3 years experienced a very different subsequent evolution, with one of the largest El Niños on record in 1998 (McPhaden 1999), a strong El Niño in late 2015, but only a weak event in late 2014 (McPhaden 2015), if one at all. Using ocean-only simulations, Menkes et al. (2014) showed that the lack of WWEs during the boreal spring

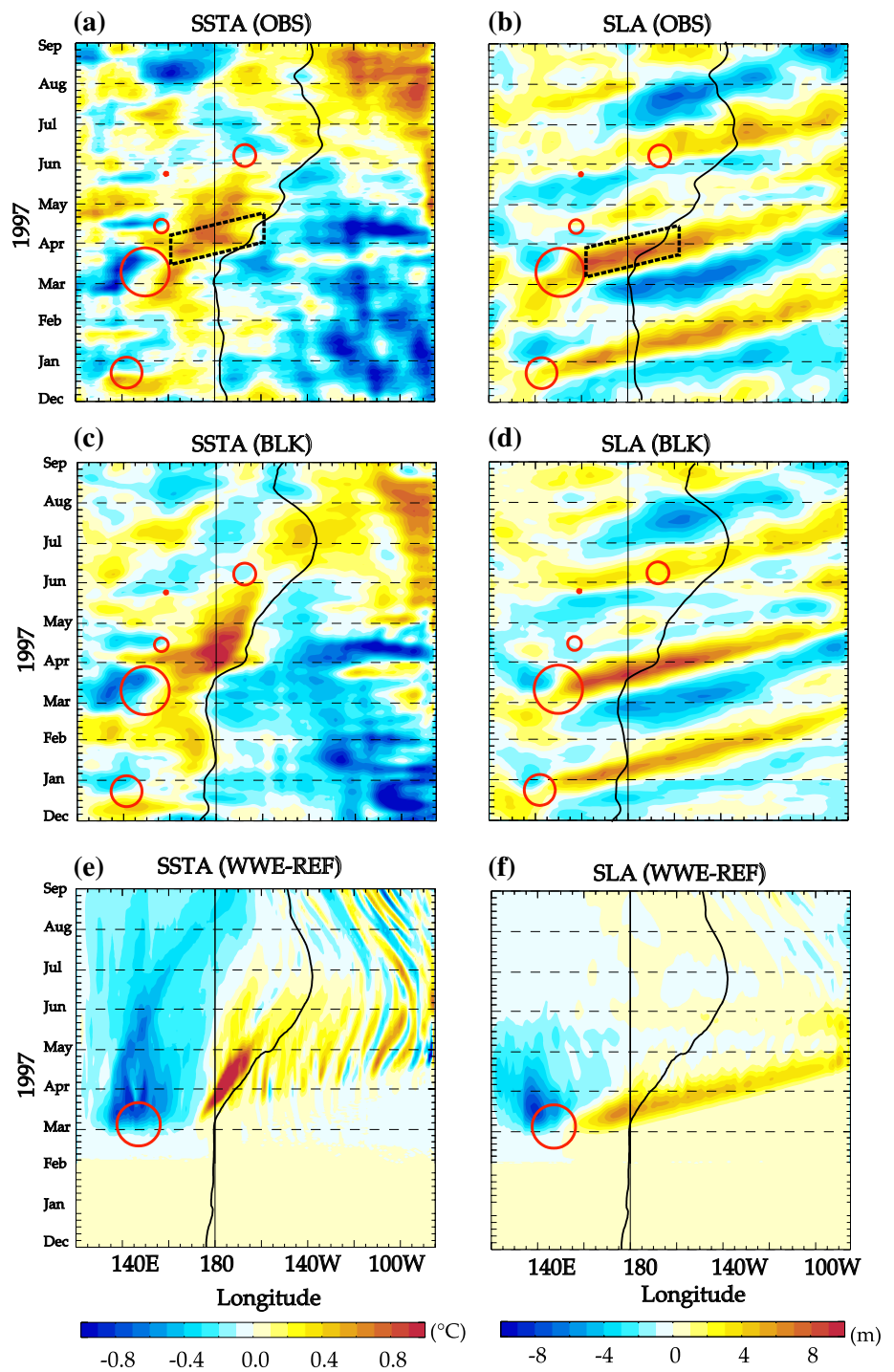
and early summer of 2014 significantly limited the growth of the warming in the equatorial Pacific, and prevented the warm event from further developing into a full El Niño. In contrast, the occurrence of several WWEs during the spring and summer of 1997 led to a major El Niño at the end of the year. A similar scenario has unrolled in 2015, leading to the strongest El Niño event since 1997. The comparison of these 3 years therefore points towards a critical role of WWEs activity for the growth of an El Niño.

WWEs impact ENSO evolution through their substantial local and remote oceanic response, which has been analysed in many observational (McPhaden and Taft 1988, 1992; Delcroix et al. 1993; Smyth et al. 1996; Feng et al. 1998; Vecchi and Harisson 2000) and modelling studies (Giese and Harrison 1991; Kindle and Phoebus 1995; Zhang and Rothstein 1998; Richardson et al. 1999; Boulanger et al. 2001; Lengaigne et al. 2002; Fedorov 2002; Drushka et al. 2015). WWEs force eastward-propagating downwelling Kelvin waves that favour a warming of the central and eastern Pacific through zonal advection in the central Pacific and/or thermocline deepening in the eastern Pacific, as illustrated on Fig. 1a, b for the onset of the 1997 El Niño event. The local oceanic response to WWEs involves a surface cooling through increased cloudiness and latent heat loss (Feng et al. 1998; Lengaigne et al. 2002) and the generation of an eastward surface jet (Belamari et al. 2003), which eventually combines with the eastward current signature of the remotely forced Kelvin wave to advect the western warm-pool warm towards the central Pacific (e.g. Boulanger et al. 2001; Lengaigne et al. 2002; Chiodi et al. 2014, Fig. 1a, b).

The Warm Pool Eastern Edge is an important region for ENSO development (e.g. Picaut et al. 2002). Small SST variations there can trigger a large atmospheric response (e.g., Palmer and Mansfield 1984; Barsugli and Sardeshmukh 2002) because the SST is close to the atmospheric convective threshold (e.g. Graham and Barnett 1987). WWEs drive a local cooling and an eastward displacement of the Warm Pool Eastern Edge (hereafter WPEE; see Fig. 1a) that indeed favour the eastward migration of deep atmospheric convection and a strong WWE activity over the western Pacific in the following months (Lengaigne et al. 2003a; Vecchi et al. 2006). This eastward displacement of the warm-pool also results in a weakening of the trade winds in the central-eastern Pacific (Lengaigne et al. 2003a, b). The trade wind weakening and the occurrence of further WWEs are hence positive atmospheric feedbacks to the initial SST response to a WWE, which will amplify the initial warming.

The SST response to WWEs is very diverse in terms of magnitude, timing and location. A large part of this diversity of course arises from the diversity of WWE characteristics such as location, intensity, fetch or duration of

Fig. 1 Time-longitude section of the 2°N-2°S average (1st column) SST and (2nd column) sea level intraseasonal (5–120 day-filtered) anomalies from December 1996 to August 1997 for **a, b** observations, **c, d** the “BLK” experiment and **e, f** the difference between the “WWE” and “CTL” experiments. On all panels, the *black line* represents the WPEE (define as the 28.5 °C isotherm) and the *red circles*, the WWEs (their size being proportional to their WEL). On **e, f** the WWE correspond to the idealized WWE added in March 1997. On **a, b** the *dotted black box* indicates the spatio-temporal domain over which the SLA and SST response shown on Fig. 3 are averaged. For the SLA response (**b**), this space-time domain starts 10° eastward of the WWE central longitude and from the WWE central date to 20 days later; and propagates 40° eastward at a 2.8 m s⁻¹ speed representative of the 1st Baroclinic Kelvin wave. The same definition is used for the SST (**a**) with a 10 days lag, to account for the lagged response of SST to the Kelvin-wave induced zonal current and thermocline depth anomalies



the WWE (Giese and Harrison 1990, 1991; Suzuki and Takeuchi 2000; Puy et al. 2016). But oceanic background conditions can also influence the response to the WWE (Schopf and Harrison 1983; Harrison and Schopf 1984; Vecchi and Harrison 2000). Several studies have for example demonstrated the sensitivity of Kelvin wave characteristics, such as zonal current anomalies or phase speed, to the mean oceanic background conditions (Gill 1982;

Busalacchi and Cane 1988; Giese and Harrison 1990; Benestad et al. 2002; Shinoda et al. 2008; Dewitte et al. 2008; Mosquera-Vasquez et al. 2014). Benestad et al. (2002) have shown that Kelvin waves excited by identical intraseasonal wind variations are strongly damped during La Niña compared to El Niño, such that little wave energy reaches the eastern coast when the mean conditions are cold. On the other hand, Shinoda et al. (2008) argued that the slowly

varying upper ocean basic state was not the primary cause of changes in Kelvin wave phase speed but rather the wind stress anomalies east of the dateline.

Overall, these studies show that the Kelvin waves characteristics are sensitive to the oceanic background state. The diversity of Kelvin waves characteristics is only one of the processes by which the oceanic state can modulate the SST response to a WWE. Only a handful of studies have however focused on the sensitivity of the WWE-induced SST response to different oceanic background conditions. Schopf and Harrison (1983) studied the oceanic response associated with the passage of downwelling Kelvin waves, using forced oceanic experiments. They found that the amplitude of the SST response to the Kelvin wave strongly depends on the oceanic conditions. The equatorial SST warming caused by the passage of the wave results from the existence of a mean negative zonal SST gradient that varies seasonally. Harrison and Schopf (1984) further argued that remotely-forced central Pacific SST changes were strongly linked to the annual variations of the SST field. They showed that similar anomalous eastward current anomalies had different SST impacts depending on the seasonal variations of the mean zonal SST gradient, with a strong impact in fall and winter when the zonal gradient is strong and a weaker impact in spring and summer. Finally, Vecchi and Harrison (2000) investigated the observed SST response to WWEs for different ENSO phases. They showed that WWEs occurring during neutral conditions drive a substantial equatorial waveguide warming in the central and eastern Pacific (up to 1°C composite warming). WWEs occurring during El Niño conditions were rather associated with the maintenance of the central and eastern Pacific warming, while these warm conditions tend to disappear in the absence of WWEs.

These studies hence suggest a strong influence of the oceanic background conditions on the ocean response to WWEs that could partly explain the diversity of the tropical Pacific response to WWEs observed during the past two decades. It is however difficult to isolate this modulation of the SST response by the ocean state in observations or even in ocean-only experiments forced by observations (Drushka et al. 2015) as the amplitude of the SST response will depend both on the WWE characteristics and the oceanic background conditions. Owing to the importance of the SST response to WWEs in the equatorial Pacific on the coupled system and more particularly on ENSO, it is important to assess the sensitivity of the WWE oceanic response to the oceanic background state and associated physical mechanisms. Our aim is here to isolate the diversity in WWE SST response associated with the oceanic background state from that associated with the diverse WWE characteristics. To that end, we use a modelling strategy in which we apply the same strong WWE (in essence

similar to the March 1997 WWE) over a realistic seasonally and interannually-varying oceanic state. The model and experimental setup are presented and briefly validated in Sect. 2. In Sect. 3, we first investigate the mechanisms that control the mean SST response in the western Pacific, at the WPEE and in the eastern Pacific. We then investigate the diversity in SST response arising from variations of the oceanic background state, along with the associated physical mechanisms and controlling oceanic variables for the same three regions. A discussion of our findings and their potential implications for ENSO predictability is finally provided in Sect. 4.

2 Data and methods

2.1 Model setup and forcing strategy

The numerical simulations in this study are performed using NEMO v3.2 (“Nucleus for European Modelling of the Ocean”) Ocean General Circulation Model, in a 1° resolution global ocean configuration known as ORCA1 (Hewitt et al. 2011). ORCA1 has a 1° nominal resolution, with a local transformation in the tropics to refine the meridional resolution to 1/3° at the equator. It has 42 vertical levels, with a vertical resolution decreasing from 10 m at the surface, to 25 m at 100 m depth and 300 m at 5000 m. The model is based on primitive equations, and uses a free surface formulation (Roulet and Madec 2000). Density is computed from potential temperature, salinity and pressure using the Jackett and McDougall (1995) equation of state. Vertical mixing is parameterized from a turbulence closure scheme based on a prognostic vertical turbulent kinetic equation, which performs well in the tropics (e.g., Blanke and Delecluse 1993; Vialard et al. 2001). Lateral mixing is applied using a Laplacian operator that acts along isopycnal surfaces, with a 200 m² s⁻¹ constant isopycnal diffusivity coefficient (Guilyardi et al. 2001; Lengaigne et al. 2003b). Shortwave fluxes penetrate into the ocean based on a single exponential profile corresponding to oligotrophic water (Paulson and Simpson 1977) with an attenuation depth of 23 m (Lengaigne et al. 2007).

The model computes its surface fluxes from specified downward shortwave and longwave radiation, precipitation, 10-m wind, 2-m air humidity and temperature, using the COAREv2 bulk formula approach (Fairall et al. 1996). Those atmospheric input variables are taken from the DRAKKAR Forcing Set v5.2 (DFS5.2, Dussin and Barnier 2013), derived from ERA 40 (Uppala et al. 2005) until 2002 and ERA-Interim reanalysis (Dee et al. 2011) afterward. All atmospheric fields are corrected to avoid temporal discontinuities and remove known biases. The model is run over the 1979–2012 period and the first year of the

experiment is discarded to allow a spin up (which takes a few months in the equatorial band). This experiment is hereafter referred to as the BLK experiment (for “Bulk” formula).

The model accurately simulates the equatorial SST mean state and seasonal cycle (not shown). This model and forcing strategy has already been shown to capture the bulk of SST variations in the tropical Pacific (see Drushka et al. 2015). An illustration of the equatorial Pacific SST variability is provided on Fig. 2a, which displays the equatorial time-longitude evolution of the TropFlux SST daily data (Praveen Kumar et al. 2012, 2013, <http://www.incois.gov.in/tropflux/>). Since the WPEE (defined here as the 28.5°C isotherm) is an important feature for ENSO development, the WPEE simulated by the BLK experiment is overlaid on the top of the observed one (blue and black curves on Fig. 2a). At interannual timescales, the model accurately captures both the observed SST variability (red curve in Fig. 2b) over the entire equatorial strip (correlation ranging between 0.8 in the western Pacific to 0.95 in the central/western Pacific) and the WPEE variability (correlation of 0.96).

We further provide some validation of the model ability to reproduce the observed response to WWEs. Because of their episodic nature (10–20 days), the observed response to WWEs predominantly occurs at intraseasonal timescales. We hence assess the ability of the BLK simulation to reproduce intraseasonal (5–120 days filtered) anomalies below. Figure 1 shows the 2°N–2°S average of those SST and sea-level anomalies during the onset phase of the 1997 El Niño in observations (Fig. 1a, b) and the BLK simulation (Fig. 1c, d). WWEs were detected using the method of Puy et al. (2016) and are indicated by red circles on this Figure. The centre of the red circles corresponds to the WWEs central dates and longitudes, while their radiuses are proportional to the Wind Event Index (WEI), also introduced in Puy et al. (2016). In essence, this index corresponds to a longitude–time integration of the zonal wind stress anomalies over the wind event patch. The index is then normalized by standard deviation, computed over all the detected WWEs, in order to obtain a dimensionless index. This index integrates the wind event amplitude, duration and zonal fetch, and is a good measure of the amplitude of the Kelvin wave forced by the WWE (Puy et al. 2016 and later in the current paper). The major WWEs in December 1996, March 1997 and June 1997 (e.g. McPhaden 1999) were all detected with our approach (Fig. 1a–d). These WWEs are all clearly related to an eastward propagating downwelling Kelvin wave signal in satellite altimetry data (Fig. 1b). In contrast, the SST response is far more diverse: an intraseasonal SST warming at the WPEE follows the March WWE, but there is no substantial SST response in this

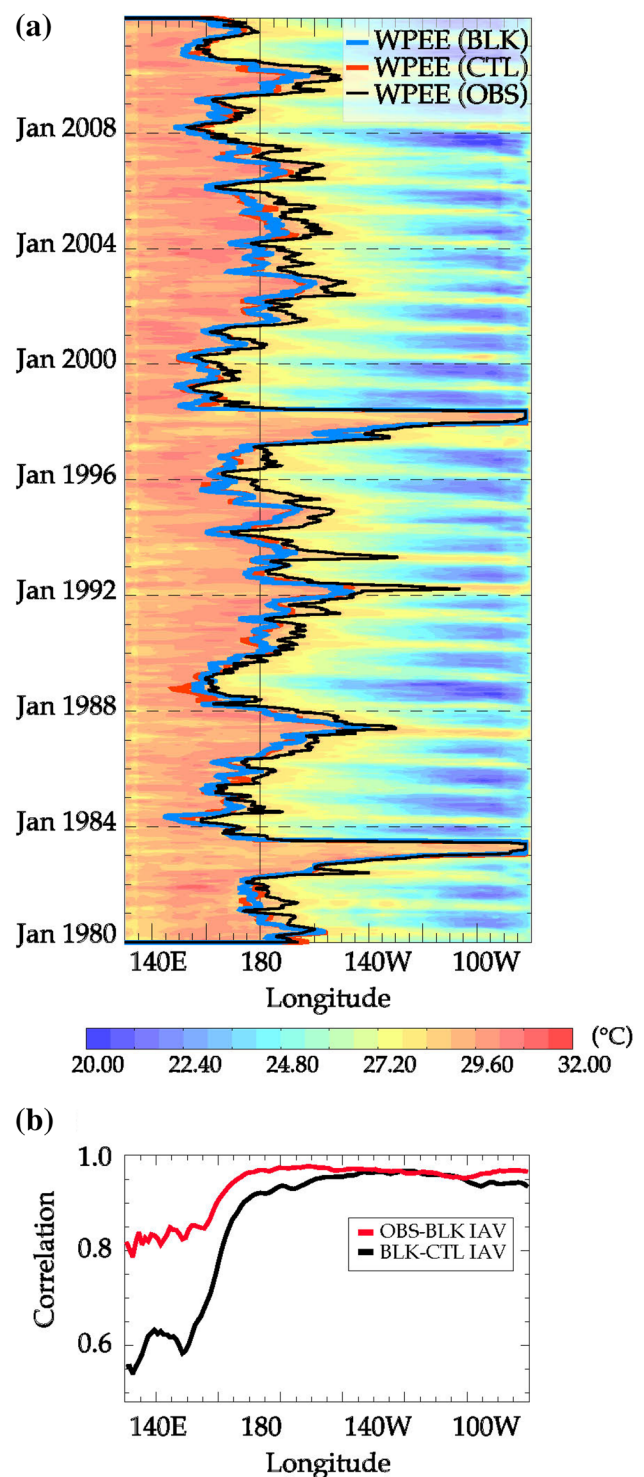


Fig. 2 a Time-longitude section of the Pacific 2°N–2°S average observed (Tropflux) daily SST over the 1980–2012 period. The thick black line represents the observed position of the Warm Pool eastern Edge (WPEE) defined as the 28.5°C isotherm. The thick red and blue lines, respectively depict the WPEE location in the CTL and BLK simulations. b Correlation of 2°N–2°S average interannual SST variations between the BLK (black)/CTL (red) simulations and observations, as a function of longitude

region to the two other WWEs (Fig. 1a). In addition, the December 1996 and March 1997 WWEs are not followed by any clear intraseasonal warming along the Kelvin wave path (rather a cooling signal), while such a warming is apparent for the June 1997 event (Fig. 1a) in better agreement with the central/eastern equatorial Pacific composite observed warming depicted by Vecchi and Harrison (2000). The most consistent SST signature amongst these three WWEs is the SST cooling under and to the west of these WWEs. This diversity is likely to arise from the fact that the intraseasonal filtering here does not capture only the response to WWEs, but also to other intraseasonal fluctuations of the air–sea fluxes.

Figure 1c, d reveals that the model captures the intraseasonal sea-level and SST signature during this period very accurately when compared to observations (“Validation_WWE-BLK_simulation” a, d). The model is thus able to reproduce the observed response to intraseasonal fluctuations in air–sea fluxes in the equatorial Pacific, including those associated with WWEs.

As pointed out earlier, Fig. 1a, b suggests a more consistent observed response of sea-level than of SST to WWEs. Figure 3a, b illustrates the statistical relationship between the WWE properties (the Wind Event Index, or WEI) and their oceanic response over the entire observational period. The WWE sea-level signature is estimated from the

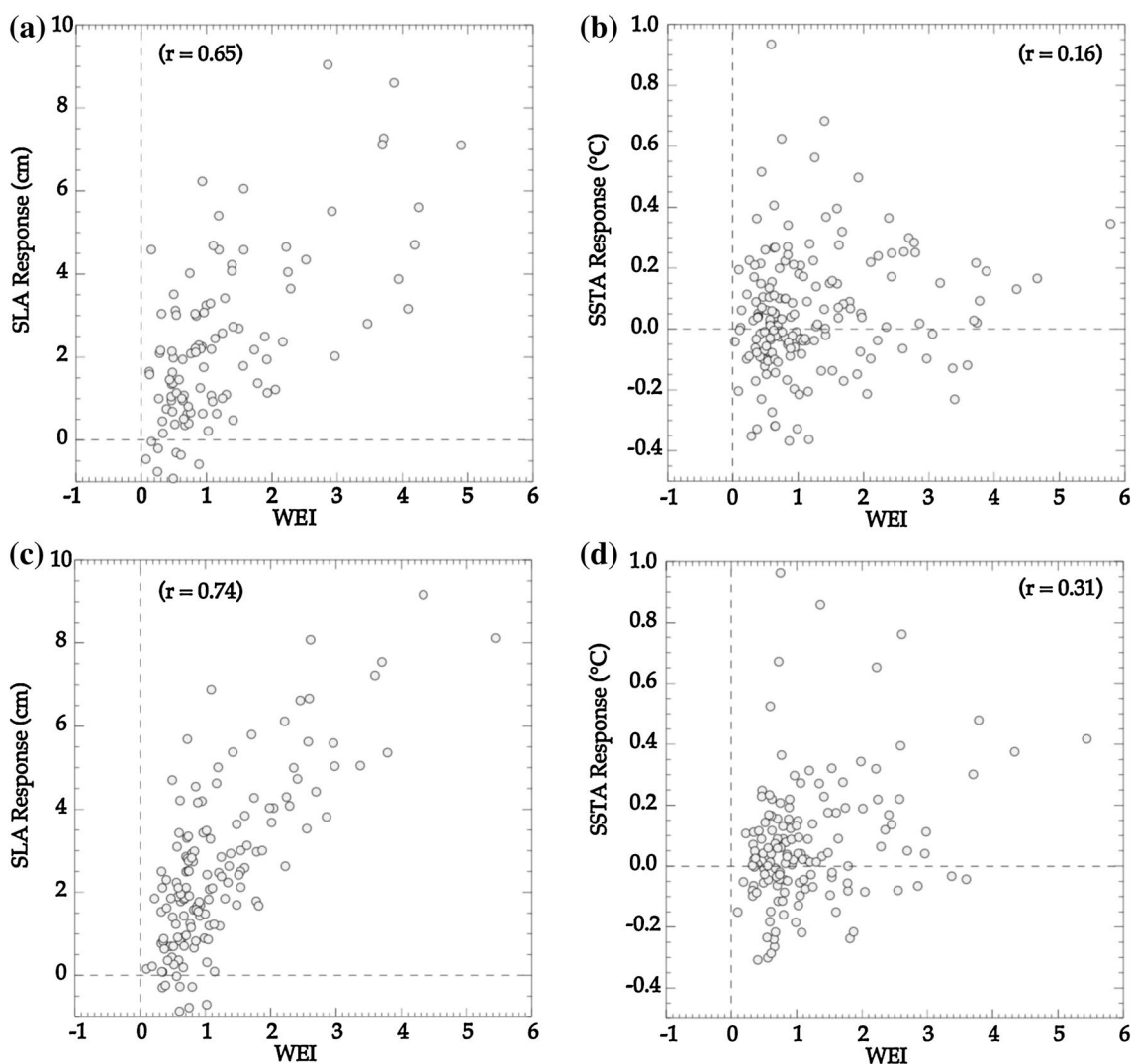


Fig. 3 a, b Scatterplot of the Wind Event Index (WEI, a longitude-time integration of the zonal wind stress anomalies over the wind event patch introduced by Puy et al. (2016), that measures the dynamical impact of the WWE on the ocean; see text for details) against the observed a sea level and d sea surface temperature anomaly responses to the WWE, averaged along the Kelvin wave path down-

stream of the wind event (An example of the spatio-temporal domain over which the SLA and SST response are averaged is shown Fig. 1a, b). c, d Similar to a, b but for the BLK experiment. In both the observation and the model, the sea level response to a WWE relates somewhat linearly to the wind event properties (a, c) while the SST response is much more diverse (b, d)

average intraseasonal (5–120 days filtered) anomaly over the space–time domain shown on Fig. 1b. This space–time domain starts 10° eastward of the WWE central longitude and from the WWE central date to 20 days later and propagates 40° eastward at a 2.5 m s⁻¹ speed representative of the 1st baroclinic Kelvin wave. This analysis shows that the sea level anomaly along the Kelvin wave path is linearly related ($r=0.65$, Fig. 3a) to the WEI. A similar analysis is provided on Fig. 3b but for the SST response. This SST response is estimated as the average in a space–time domain (shown on Fig. 1a) that is shifted 10 days later relative to that used for sea level, in order to account for the lagged response of SST to the Kelvin-wave induced zonal current and thermocline depth anomalies (results are insensitive to using a 0–20 day lag). In contrast to sea level, and as already suggested by the case study of Fig. 1, the SST response to the wind event cannot easily be related to the wind event characteristics ($r=0.16$ Fig. 3b). The BLK simulation also exhibits a similar behaviour as shown on Fig. 3c, d: the modelled sea level anomaly along the Kelvin wave path is of the same magnitude as in the observation and is also linearly related to the WWEs characteristics ($r=0.74$, Fig. 3c) while the SST anomalies are poorly related to the WEI ($r=0.31$, Fig. 3d). This is an indication that the SST response to the wind event cannot simply be related to the wind event characteristics and that the oceanic conditions have to be taken into account, as discussed in the introduction.

2.2 Idealized WWE forcing

As our goal is to assess the sensitivity of the WWE response to varying oceanic background conditions, we choose to analyse the ocean model response to the same WWE applied over a varying oceanic background state. Below, we explain how we constructed this idealized WWE forcing, based on observed WWE air–sea flux anomalies.

WWEs momentum and heat flux signatures are derived from the Tropflux air–sea flux product that shows one of the best agreements with TAO-mooring data (Praveen Kumar et al. 2012, 2013). TropFlux equatorial zonal wind stresses in particular exhibit the best phase agreement with TAO mooring data at intraseasonal timescales over the western and central Pacific (above 0.95 correlation) and reproduce the WWE wind stress signature that played a key role in the 1997–1998 El Niño onset best (Praveen Kumar et al. 2012). Regarding heat flux, Tropflux also performs best, with a similar amplitude and a ~ 0.85 correlation with TAO moorings data over the Pacific warm pool (Praveen Kumar et al. 2013). This product still exhibits a ~ 25 W m⁻² rms-difference with TAO mooring data in this region, a value that can hence be considered as the typical heat flux error associated with the WWEs signature.

We built an idealized WWE forcing from the 10% strongest WWEs as measured by their WEI (corresponding to 20 WWEs over the period). Figure 4a, e show the equatorial time–longitude evolution of the zonal wind stress and net heat flux anomalies of this WWE composite. This composite exhibits westerly wind stress anomalies of up to 0.1 N m⁻² lasting for more than 10 days with a typical zonal extension of $\sim 30^\circ$ and oceanic heat losses of up to -90 W m⁻² with a similar contribution from the solar and non-solar (mainly latent heat fluxes) components (not shown). The amplitude of this heat flux signature is within the range of the one depicted by measurements under WWE conditions monitored during the COARE period (~ 100 W m⁻²; e.g. Smyth et al. 1996; Cronin and McPhaden 1997). The two strongest WWEs on record in terms of WEI occurred in December 1996 and March 1997 and are displayed for comparison on Fig. 4b, c, f, g. Although their wind stress anomalies are 50% stronger (~ 0.15 N m⁻²), they exhibit a similar duration (10–20 days) and zonal extent ($\sim 30^\circ$) to those of the composite. They however reveal a stronger diversity in terms of heat flux response, with negative anomalies reaching -180 W m⁻² in December 1996 and weaker anomalies, above -50 W m⁻², in March 1997. Although there is a general tendency for intense WWEs to be associated with large net heat flux anomalies (not shown), the heat flux response to strong WWEs varies considerably (the strongest 20% are associated with heat flux anomalies equal to -75 W m⁻² on average with a standard deviation of 30 W m⁻²). We will discuss the consequences of this diversity in Sect. 4.

Based on the composite for strong WWEs, we build an idealized WWE surface momentum and heat flux perturbation (Fig. 4d, h). We choose a temporal and spatial Gaussian shape for both the zonal wind stress and net heat flux as follows:

$$\begin{pmatrix} \tau_{idl} \\ Q_{idl} \end{pmatrix}(x, y, t) = \begin{pmatrix} \tau_0 \\ Q_0 \end{pmatrix} \cdot e^{-\left(\frac{t^2}{\sigma_t^2} + \frac{x^2}{\sigma_x^2} + \frac{y^2}{\sigma_y^2}\right)}, \quad (1)$$

where τ_0 (0.1 N m⁻²) and Q_0 (-180 W m⁻²) represent the maximum magnitude of the zonal wind stress and net heat flux during the events, and σ_t , σ_x and σ_y are respectively the time (10 days), zonal (10°) and meridional (4°) scales of the WWE. With such values, the WEI of this idealized WWE is 3.0, close to the WEI of the March 1997 and December 1996 WWEs (3.4 and 3.2, respectively) and the idealized heat flux anomalies are consistent with those monitored for some of the largest observed WWEs.

The idealized WWE is added in the western Pacific, between 140 and 150°E, in a region where WWEs are frequently observed (50% of observed WWEs; Puy et al. 2016) and where the two strong events discussed above occurred. As suggested by Tropflux data, the heat flux

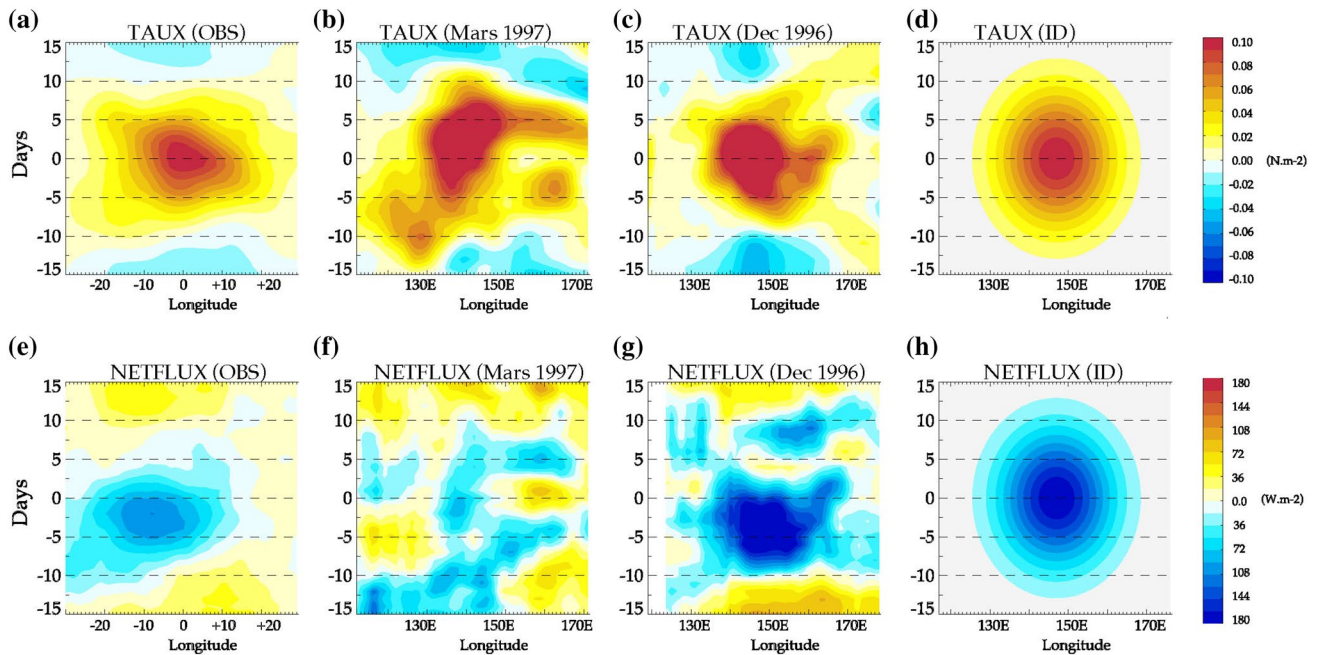


Fig. 4 Time-longitude section of the 2°N – 2°S average of (*top*) surface wind stress and (*bottom*) net surface heat flux perturbations associated with (*1st column*) a composite based on the 10% strongest WWEs (20 events over the 1979–2012 period), (*2nd column*) the

March 1997 WWE, (*3rd column*) the December WWE and (*4th column*) the idealized WWE applied in our “WWE” sensitivity experiments

signature is split equally onto the solar and non-solar heat flux components when applied in the ocean model.

2.3 Sensitivity experiments design

We want to apply the idealized WWE forcing described above at different periods in the reference simulation, which exhibits seasonally and interannually varying oceanic background conditions close to that of observations (Fig. 2). There are, however, two potential issues in doing so. First, although there is no explicit relaxation to observed SST in the BLK experiment where fluxes are computed using bulk formulae, the specification of the air temperature and humidity implies an implicit restoring term, which will tend to damp the SST response to WWEs (Drushka et al. 2015). Second, the BLK experiment already contains high frequency variability (and in particular WWEs) and adding an idealized WWE on top of a pre-existing WWE may blur the analysis. In order to circumvent these two issues, we perform an additional control experiment (referred to as CTL experiment in the following) forced by intraseasonally filtered (using a triangle low-pass filter with a cut-off period of 90 days) heat, momentum and freshwater flux forcing from the BLK experiment. Only a modest SST relaxation to the BLK climatology (180 days timescale for a 40 m-thick mixed layer) is used in the CTL simulation to avoid any potential drift. This CTL experiment displays a

very similar WPEE displacement compared to that of the BLK experiment (Fig. 2a; ~ 0.96 correlation) and very similar interannual equatorial SST evolution (Fig. 2b), except west of 160°E . In the western Pacific, the interannual SST variations are small ($\text{STD}=0.29^{\circ}\text{C}$) compared to the rest of the equatorial Pacific ($\text{STD}=1.15^{\circ}\text{C}$), hence small differences between the observation and the model lead to a stronger signal to noise ratio that degrade the correlation.

The idealized WWE forcing described in Sect. 2.2 is then added to the CTL atmospheric forcing every 5th of March, June, September and December of each calendar year over the 1980–2011 period (i.e., 124 WWEs in total). This strategy allows sampling very contrasted but realistic oceanic background conditions at seasonal and interannual timescales (the entire range of ENSO conditions are thus sampled). We first verify if the applied WWEs in our experiment are consistent with the observed distribution of WWEs occurring in the western Pacific. To that end, Fig. 5a, b compares the observed western Pacific WPEE distribution and Niño3 SST anomaly for all western Pacific WWEs (119 events detected over the period 1980–2012) to that associated with the 124 regularly-spaced WWEs in our idealized experiment. Figure 5a clearly shows that the two distributions are similar, except for four idealized WWEs that were applied in the western Pacific during mature phases of extreme El Niño (December 1982, March and June 1983 and December 1998, when the warm pool stands

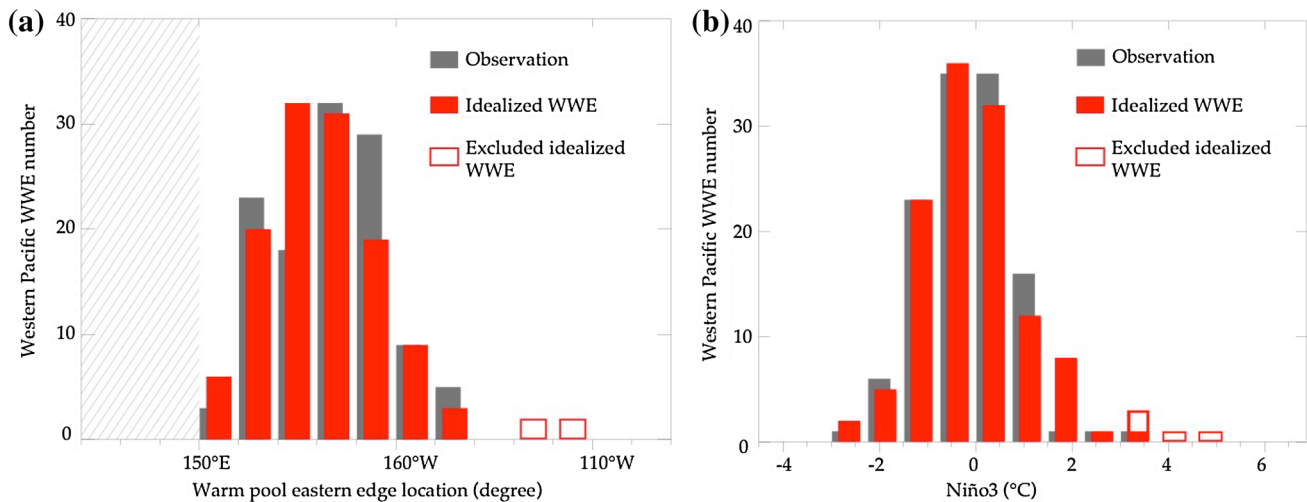


Fig. 5 Distribution of **a** the Warm Pool eastern Edge (WPEE) location and **b** the Niño3 SSTA anomaly for observed Western Pacific (120–150°E, indicated by the grey stippling) WWEs (grey) and for the western Pacific WWEs in our idealized WWE (red). Applying

WWEs at regular intervals would result in some unrealistic WWEs (WWEs during fully developed ENSO events, shown here as red boxes with no filling), which are not observed; those WWEs were hence excluded from all the statistics shown in this paper

further east of 130°W), a feature that is not observed. Figure 5b further shows that the distribution of the idealized WWEs regarding ENSO phases is quite realistic, with the majority of the events occurring during neutral ENSO state [55% comparing to 61% in the observation, when the SST anomaly in the Niño3 region ranges between the interval (−0.75; 0.75 °C)]. Also, 24% occurs during La Niña (compared to 20% in the observation when the SST anomalies in the Niño3 region are colder than −0.75 °C) and 21% during El Niño conditions (compared to 19% in the observation when the SST anomalies in the Niño3 region are warmer than 0.75 °C). The four unrealistic WWEs (based on the WPEE location, Fig. 5a) are also highlighted on Fig. 5b and correspond to events occurring when the Niño3 SST anomaly are larger than 3.5 °C. These unrealistic WWEs have hence been excluded from all the diagnostics of the present study, which are based on the remaining 120 WWEs (this removal does not however change the main conclusions of the present study).

Adding these successive WWEs over the course of a single simulation would result in a cumulative WWE response and hence a mean state change, which would prevent isolating the effect of a single WWE from the cumulated impact of the previous ones. For each WWE, we therefore perform a 1-year long simulation starting from the CTL initial state 1 month before the WWE is applied. This strategy results in 120 (4 times 31 years minus the four unrealistic events) 1-year long simulations that can directly be compared to the CTL simulation to assess the oceanic response to WWEs under the varying oceanic background conditions over the 1980–2011 period. The oceanic response to a given WWE is simply

computed by performing the difference between these “WWE” experiments and the CTL simulation. In order to illustrate this approach, Fig. 1d, f illustrates the diagnosed SST and sea level response to the March 1997 WWE. In qualitative agreement with observations and BLK simulation, this WWE is associated with a clear eastward propagating Kelvin wave signal (Fig. 1f), a cooling below the WWE and warming along the WPEE (Fig. 1e) during the 2 months following the event. The amplitudes of the signals are however different because the idealized WWE is characterized by a WEI slightly weaker than the one of March 1997 WWE (3 compared to 3.4) and much larger negative heat flux anomalies (−180 W m^{−2} compared to −50 W m^{−2}). However, our idealized setup reveals a clear warming along the Kelvin wave path in the central and eastern Pacific, which is not obvious in either observations or the BLK simulation intraseasonal anomalies, which mix the WWE response to that of any other source of intraseasonal forcing. This example hence clearly illustrates the added value of conducting this idealized setup to clearly isolate the oceanic response to WWE forcing.

The mean composite and the diversity of the WWE response are then computed as the mean and the standard deviation of the difference between the runs with the WWE minus the CTL simulation, for the 120 idealized WWEs. For the sake of brevity, we will refer to this collection of simulations as “the” WWE simulation. Using an identical idealized WWE forcing superimposed onto seasonal and interannual varying oceanic background conditions allows exploring the sensitivity of the WWE oceanic response to the seasonal cycle and ENSO conditions.

2.4 Heat budget

The processes that control the SST response to WWEs are characterized using an online mixed layer heat budget calculation. The budget equation for the average temperature over the time varying mixed layer \mathbf{T} (a proxy for the SST) reads as follows (e.g., Vialard et al. 2001):

$$\partial_t \mathcal{J} = + \underbrace{\frac{Q_s(1-f|_{-h}) + Q^*}{\rho C_p h}}_{For} - \underbrace{\int_{-h}^0 u \partial_x T dz - \int_{-h}^0 v \partial_y T dz}_{Had} - \underbrace{\frac{(\kappa \partial_z T)|_{-h} + \left(w|_{-h} + \frac{dh}{dt}\right)(T|_{-h} - \mathcal{J})}{h}}_{Ver} + \underbrace{\int_{-h}^0 D(T) dz}_{Ldf} \quad (2)$$

where h is the time-varying model mixed layer depth estimated based on a potential density increase of 0.01 kg m^{-2} relative to the surface, Q_s and Q^* are respectively the solar and non-solar components of the surface heat flux, $f|_{-h}$ the fraction of incoming solar radiation that penetrates below the mixed layer, ρ the seawater density, and C_p the sea water volumic heat capacity. The term “*For*” represents the heating rate of the mixed layer associated with the effect of air-sea fluxes (that will be referred to as “atmospheric forcing” in the following, for the sake of simplicity). (u , v , w) are the components of the current and the term “*Had*” hence represents the horizontal (zonal and meridional) temperature advection in the mixed layer. κ is the vertical tracer mixing coefficient, so $\kappa \partial_z T|_{-h}$ represents turbulent mixing at the bottom of the mixed layer, $w|_{-h} (T|_{-h} - \mathbf{T})$ represents the effect of upwelling and $\frac{dh}{dt} (T|_{-h} - \mathbf{T})$ is the entrainment of deeper water into the mixed layer, which is computed as the budget residual. The term “*Ver*” hence represents the exchanges between the mixed layer and the interior ocean (upwelling and turbulent processes) and is referred to as “vertical processes” in the following. The term “*Ldf*” is the lateral mixing and is always negligible in the present analysis.

3 Modulation of the WWE response by the background oceanic state

In this section, we first present an overview of the average oceanic response to WWEs applied in the sensitivity experiment and of the spread due to the varying oceanic background conditions (Sect. 3.1). We then investigate the mechanisms of the mean response and of its diversity in more details in the western Pacific (Sect. 3.2), near the warm pool eastern edge (Sect. 3.3) and in the eastern Pacific (Sect. 3.4).

3.1 Overview of the mean response to a WWE

Figure 6a–c displays the equatorial longitude-time evolution of the composite oceanic response averaged over the 120 WWEs applied in the sensitivity experiment. The response is consistent with previous literature (see Lengaigne et al. 2004a, b for a review) in terms of SST (Fig. 6a,

cf. Smyth et al. 1996; Cronin and McPhaden 1998; Lengaigne et al. 2003a, b), surface currents (Fig. 6b) and thermocline depth (Fig. 6c, cf. Boulanger and Menkes 1999; McPhaden 2002).

Under the WWE forcing, the western Pacific is characterized by a cooling of up to -1°C 15 days after the WWE occurrence (Fig. 6a), a strong eastward surface jet exceeding 0.8 m s^{-1} locally (Fig. 6b), and a westward-propagating negative thermocline depth anomaly (taken here as the 20°C isotherm depth and referred to D20 in the following) signal consistent with an upwelling Rossby wave signal (Fig. 6c). Further east, the WWE drives a downwelling Kelvin wave response, associated with a 16 m deepening of the D20 and a 0.2 m s^{-1} anomalous eastward current along its path (Fig. 6b, c). This Kelvin wave signal propagates eastward from the WWE forcing region at an average phase speed of 2.8 m s^{-1} . This downwelling Kelvin wave is also associated with a warming near the dateline, corresponding to a WPEE eastward displacement, and with a warming along the Kelvin wave path. This warming is intensified in the eastern Pacific, where the mean thermocline is shallower, and reaches 1°C 2 months after the WWE.

Figure 6d–f further provides a measure of the spread around this mean ocean response to the WWE, measured from the standard deviation of the 120 WWE responses comprising the composites on Fig. 6a–c. The applied idealized WWE being identical over the course of the WWE experiment, the spread in the oceanic response can be directly attributed to the modulation by background oceanic conditions. This spread is rather weak in terms of zonal current (standard deviation of $\sim 0.1 \text{ m s}^{-1}$ under the WWE) and thermocline depth (standard deviation ranging from 2 m along the Kelvin wave path to 6 m in the eastern Pacific) response (Fig. 6e, f), representing a $\sim 20\%$ deviation of the mean response (Fig. 6b, c). This modest sensitivity is in agreement with the fact that the WWE intensity correlates well with the observed sea level response (cf. Fig. 3a) and that the linear equatorial wave theory applies well to the sea level response to

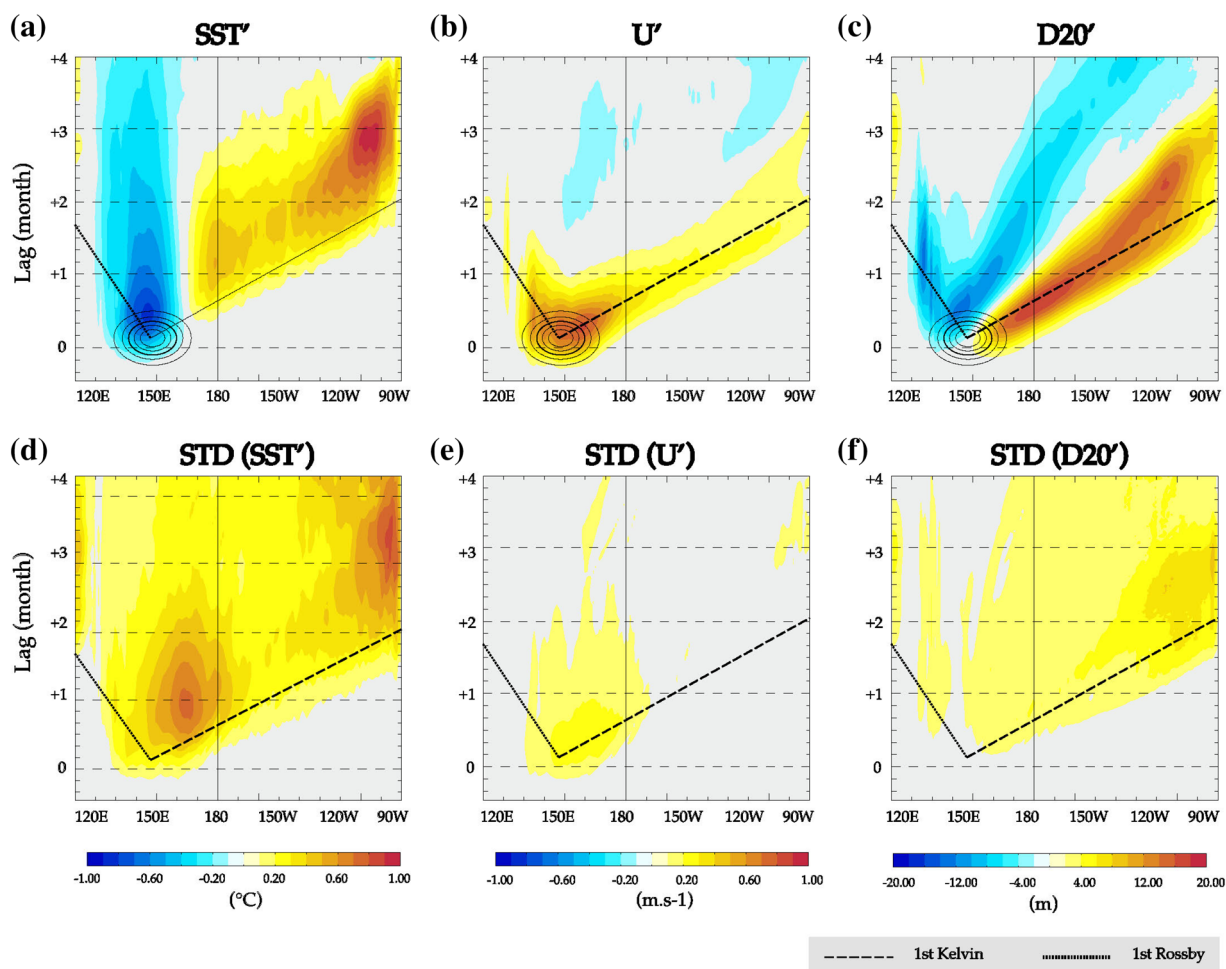


Fig. 6 (1st row) Time-longitude section of the 2°N-2°S average of a composite of **a** SST, **b** zonal current and **c** Depth of the 20°C isotherm (D20) response to the 120 westerly wind events applied in the WWE sensitivity experiments. The solid contours on panel **a** display the idealized structure of the wind stress and net heat flux perturbations added in the WWE experiments [contour interval of 0.02 N m⁻²/30 W m⁻²]. (2nd row) Sensitivity of the **d** SST, **e** zonal current and **f** D20 response to the variability in oceanic background

conditions, measured from the standard deviation of the 120 WWE-induced simulated response. *Red* contours on panel **a** represent the *three boxes* (West, WPEE for Warm Pool Eastern Edge, and East) that we use in the following figures. The WPEE box is centered on the longitude of the Warm Pool Eastern Edge (i.e., it is a moving box centered on the 28.5°C isotherm). The *dashed (dotted) lines* indicate the theoretical 1st baroclinic Kelvin (1st meridional mode Rossby) waves phase speed

wind anomalies in the equatorial Pacific. In the Sect. 4.2 section, we will show that this modest modulation of the Kelvin wave characteristics by the background oceanic state agrees with previous studies (e.g. Benestad et al. 2002). The SST response to the WWE is far more sensitive to the oceanic background conditions than its dynamical response, with a spread of the same order of magnitude as the mean response (Fig. 6d versus a), especially at the WPEE and in the eastern Pacific. The SST response to the WWE is now detailed in three regions of interest: below the WWE in the western Pacific (130°E: 160°E, Sect. 3.2), in a moving 10° wide box centered on the WPEE (Sect. 3.3) and in the eastern Pacific (120°W: 90°W, Sect. 3.4).

3.2 The western Pacific region

Small SST perturbations over the warm pool region can have a strong impact on deep atmospheric convection and hence induce a large atmospheric response (e.g., Palmer and Mansfield 1984; Barsugli and Sardeshmukh 2002). It is thus crucial to understand the mechanisms that control the amplitude of the SST response there. We first investigate the mechanisms responsible for the mean WWE-induced cooling in the western Pacific and then explore how background oceanic conditions modulate this mean cooling.

Figure 7 shows the composite of time-cumulated mixed layer temperature budget for the averaged response to WWEs in the western Pacific. These budget terms have

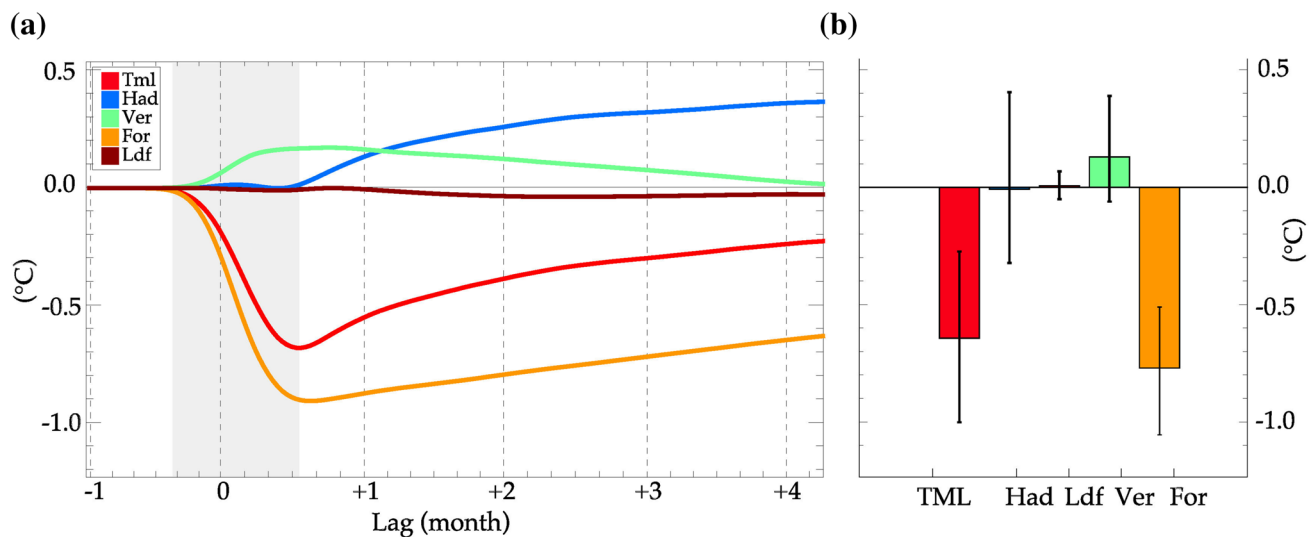


Fig. 7 Time-cumulated mixed layer heat budget terms associated with the SST composite response to the WWEs in the western Pacific region: **a** Composite time series and **b** composite decomposition of the WWE SST response into various physical processes at the time of the peak SST anomaly. This composite is based on the WWE minus CTL experiments for 120 idealized WWEs (see text for details). The *whiskers* on **b** indicate the 5th and 95th percentiles of the 120 WWE-induced simulated response from which the composite

response is constructed. The *grey shading* on **a** indicates the period over which the Time-cumulated mixed layer heat budget terms shown on **b** were computed. The mixed layer temperature anomaly is referred as “TML”. “Had” stands for the horizontal advection anomaly, “Ldf” represents the lateral mixing anomaly, “Ver” the vertical processes anomaly and “For”, the heating rate anomaly associated with the effect of air–sea fluxes. All the anomalies were computed as the difference between the “WWE” and “CTL” experiments

been integrated in time starting from the WWE occurrence and the red curve hence corresponds to the total WWE-induced cooling in this region. The SST cools down quickly, reaching -0.7°C at the end of the WWE forcing and then warms up more gradually (red curve in Fig. 7a). This quick cooling is largely dominated by the atmospheric forcing term and slightly damped by vertical processes (presumably because the surface cooling reduces the vertical gradient at the base of the mixed layer). The atmospheric heating term is negative during the first month, around the WWE central date, due to the negative surface heat fluxes imposed together with the wind pattern (-60 W m^{-2} on average over the western Pacific box) and damped by the WWE-driven mixed layer deepening from 20 m in the reference experiment to 40 m on average in the WWE experiment (not shown). The subsequent gradual decay of the cold anomaly is driven by atmospheric forcing, due to the weak relaxation to climatology applied in the simulation, and by the mean horizontal advection that progressively acts to “refill” the WWE-induced cold patch with adjacent warmer western Pacific waters.

The WWE-induced average cooling in the western Pacific is hence mostly driven by the direct effect of the WWE-induced heat fluxes. *Whiskers* on Fig. 7b illustrate the spread of the various mechanisms driving this mean SST response (i.e., the 5th and 95th percentiles associated with each term). They show that the amplitude of this cooling exhibits considerable fluctuations around its average

value depending on background oceanic conditions, ranging from -0.1 to -1.2°C , hence resulting in an order of magnitude difference between the strongest and weakest cooling. While horizontal advection does not contribute to the mean cooling, it also exhibits strong variations due to changes in oceanic background state (from -0.4°C to 0.7°C), as do vertical processes and atmospheric forcing (see whiskers on Fig. 7b). Figure 8 allows identifying which of these three processes mainly controls the diversity in the SST response, by providing scatterplots between the WWE SST response and cumulated horizontal advection (Fig. 7a) and atmospheric forcing (Fig. 7b). The vertical processes (not shown) contribute in a negligible way to both the mean and the diversity of the SST response. While horizontal advection does not contribute to the mean cooling (Fig. 7b, dashed vertical line on Fig. 8a), it controls most of its variations, with a 0.83 correlation (Fig. 8a) and 0.8 regression coefficient to the total SST anomaly (Table 1). In contrast, while the atmospheric forcing term drives the mean cooling (mean value close to -0.8°C , dashed vertical line on Fig. 8b), it does not contribute to its diversity (0.11 correlation and -0.09 regression coefficient to WWE-driven SST anomalies, Fig. 8b; Table 1). This large spread of the atmospheric forcing term can largely be attributed to variability in the background mixed layer depth just before the WWE (not shown). It doesn’t affect the SST variability because there tends to be a cancellation between the mixed layer heating due to air–sea fluxes and

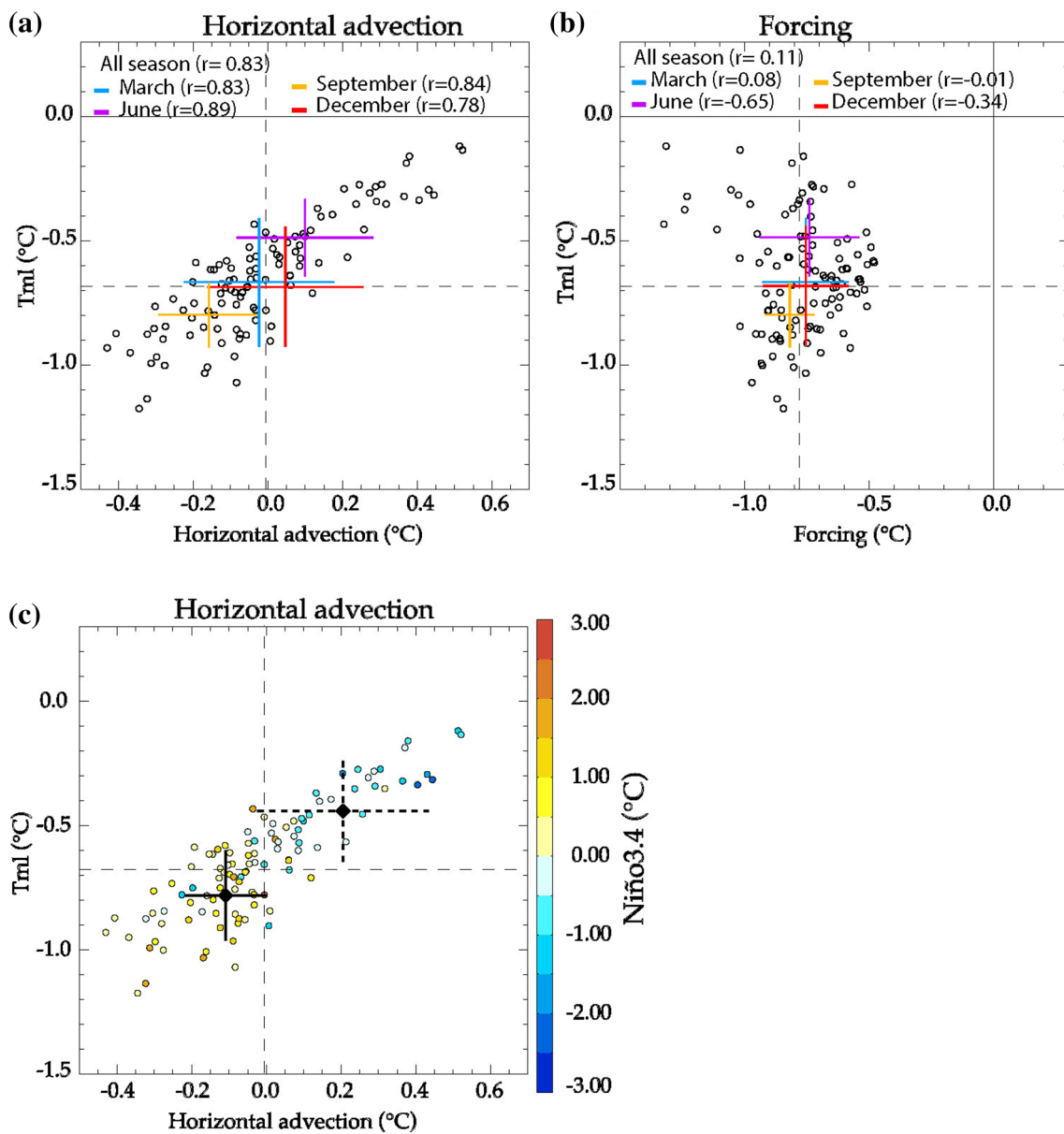


Fig. 8 Scatterplot of **a** horizontal advection and **b** atmospheric forcing contribution against the SST response to the WWE, at the time of the peak SST anomaly in the western Pacific region for each of the 120 applied WWEs. The *dashed lines* on **a**, **b** indicate mean values. The *coloured crosses* indicate the mean values individually for each of the four different seasons, with the length of each arm of the *cross* indicating the standard deviation. The correlation between the paired variables are given on the *top left* of each panel both for the whole year and individual seasons. **c** Scatterplot of horizontal advection contribution against the WWE-induced SST response for each of

the 120 WWEs. The *color* represents the values of the standardized average SST interannual anomalies in the Niño3.4 region during the occurrence of each WWE. The *black dots* and *crosses* show the mean and the associated standard deviation for the WWE occurring during El Niño conditions (*full line*) and La Niña conditions (*dashed line*). We consider that a WWE occurs during El Niño (La Niña) conditions when the value of the ENSO index (computed as the standardized average interannual SST anomalies in Niño3.4 region) is above 0.5 °C (below -0.5 °C)

the exchange between the mixed layer and the underlying ocean. This cancellation is due to the fact that a larger negative heat flux creates a stronger vertical thermal stratification that will enhance cooling by vertical turbulent fluxes.

To further isolate which component of the anomalous horizontal advection term is responsible for the diversity

of the SST response to WWEs, we decompose the zonal advection term into its background (i.e. the value in the CTL run, where no WWE is applied, noted \bar{X}) and WWE response (the WWE minus CTL difference noted X') components. We focus on zonal advection since the meridional advection contributes weakly to the total horizontal

Table 1 Contribution of each tendency term to the WWE-induced mixed layer temperature anomaly at the time of the maximum anomaly in the West, near the Warm Pool Eastern Edge (WPEE) and East. This number has been obtained by regressing each of the time-integrated tendency terms to the SST anomaly

	Had	Ldf	Ver	For
West	0.80	-0.07	0.36	-0.09
WPEE	1.11	0.04	0.06	-0.21
East	0.21	-0.1	1.23	-0.34

advection (regression coefficient of 0.3 to the horizontal advection):

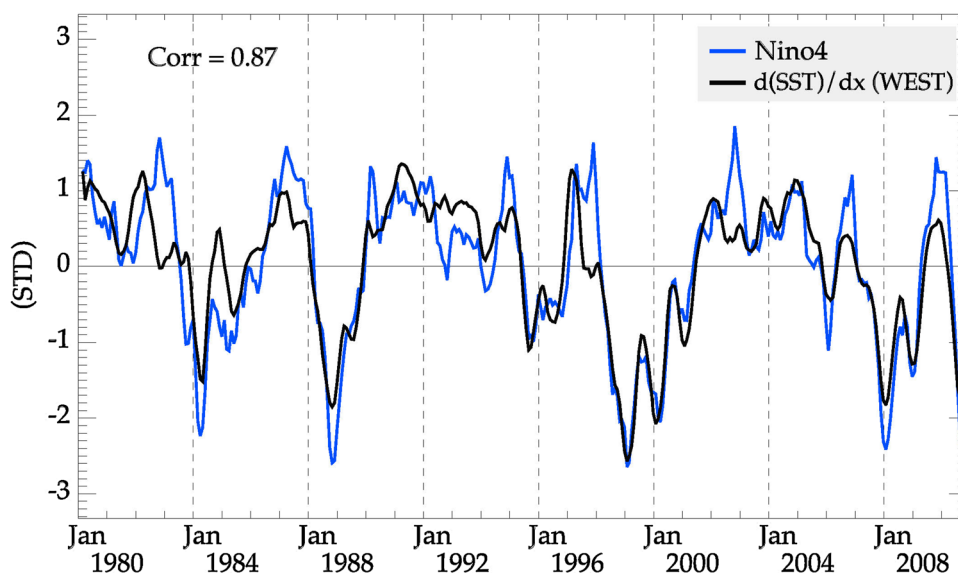
$$-(uT_x)' = -u'\bar{T}_x - \bar{u}T'_x - u'T'_x. \quad (3)$$

The first term on the right hand side contributes the most to the WWE-induced zonal advection (regression of 1.02 to the left-hand-side, against 0.16 and -0.18 for the two other terms). The advection of the background zonal SST gradient by WWE-induced currents is thus the main source for the diversity in WWE-induced SST anomalies. As shown by Fig. 6e, the current response to the WWE (u') does not vary considerably (standard deviation of 0.1 m s^{-1} for a mean values of 0.45 m s^{-1}). The sign and magnitude of the WWE-induced advection of temperature will thus vary depending on the background SST gradient in the western Pacific \bar{T}_x when the WWE occurs. The $-u'\bar{T}_x$ correlation with the WWE-induced current anomaly u' is 0.05 while it is -0.92 with the background SST gradient \bar{T}_x . This results in a correlation of -0.7 between the WWE-induced maximum cooling T' and background SST gradient in the western Pacific. A negative background SST gradient (warmer water to the west) will indeed result in a warming of the western Pacific

box through horizontal advection of the WWE-induced zonal current, hence attenuating the effects of the WWE-induced negative heat fluxes.

The western Pacific background SST gradient is dominated by interannual variations: the regression coefficient of the interannual component to the total SST gradient reaches 0.77 and the standard deviation of the interannual SST gradient is twice larger than that of the seasonal cycle. The diversity of the WWE-induced western Pacific SST cooling hence only exhibits small seasonal variations (coloured crosses in Fig. 8a–b) with a maximum 0.3°C variation between June and September, while the total cooling diversity ranges between -0.1 and -1.2°C . The western Pacific background SST gradient is strongly correlated with the Niño4 ENSO index (0.87, Fig. 9). One thus expects a strong control of the western Pacific WWE-induced SST response by ENSO. Figure 8c displays a similar scatterplot to Fig. 8a (horizontal advection contribution against the WWE-induced SST cooling in the western Pacific), colour-coded with the synchronous Niño 3.4 interannual SST anomaly. La Niña conditions (Niño 3.4 index $< -0.5^\circ\text{C}$) yield a weak WWE-induced cooling (-0.4°C on average), because warmest water during La Niña are confined to very western Pacific and Indonesian region, resulting in a negative zonal SST gradient below the WWE thus inducing a warming contribution from horizontal advection (0.25°C on average). During El Niño conditions, the warmest waters are shifted eastward into the central Pacific, resulting in a positive zonal SST gradient below the WWE and thus a cooling contribution from horizontal advection that strengthens the surface-flux induced SST cooling, with a twice as large cooling (-0.8°C on average). The implications of this ENSO control on the WWE-driven western Pacific SST response will be discussed in Sect. 4.

Fig. 9 Time series of the zonal SST gradient in the western Pacific (black) and Niño4 average SST interannual anomalies (blue) in the CTL simulation



In this section, we have shown that the WWEs locally cool the western Pacific through the heat losses they induce at the air–sea interface. The amplitude of this mean response can however vary by one order of magnitude under the effect of the advection of the background zonal SST gradient by the WWE-induced current anomalies. A positive SST gradient (warmer water to the west, typical of La Niña conditions) will be associated with a warming by the WWE-induced transport that will limit the overall cooling (with the potential to fully offset it in presence of a strongly positive SST gradient). As a result, the amplitude of the WWE-induced cooling is correlated at 0.7 with the background SST gradient.

3.3 The WPEE region

The Warm Pool Eastern Edge is also an important region for ENSO development (e.g. Picaut et al. 2001). As for the western Pacific, we first investigate the mechanisms responsible for the mean WWE-induced warming at the WPEE and then explore how background oceanic conditions modulate this mean warming. Note that similar results are obtained if the fixed Niño four region is considered, although with a weaker amplitude SST response, since the maximum SST response to WWE is almost always close to the WPEE.

Figure 10 shows the same analysis as Fig. 7, but for a region centred on the longitudinally-moving WPEE. The WPEE region starts warming 5–15 days after the WWE occurrence (Fig. 10a), consistent with the time it takes for the Kelvin wave signal to propagate there (see Fig. 6b, c). The warming increases to a maximum of 0.7 °C 1 month after the WWE, and then slowly decays back to zero over

the next 2 months. The warming and cooling phases are both dominated by the horizontal advection (Fig. 10a). The atmospheric forcing tends to cool the ocean surface (Fig. 10a), initially through the WWE-induced negative heat fluxes and later through the restoring term (not shown). The vertical processes tend to balance the negative contribution of the atmospheric forcing (Fig. 10a), as a result of the stratification increase in response to the mixed layer warming (not shown).

Whiskers on Fig. 10b illustrate the spread of the various mechanisms driving this mean SST response (i.e., the 5th and 95th percentiles associated with each term). As in the western Pacific, the varying background oceanic conditions drive a WWE SST response that ranges from 0.2 to 1.6 °C, i.e., an order of magnitude difference between the strongest and weakest warming. All the contributing processes exhibit a strong variability, except lateral diffusion (Fig. 10b). Variations in the WWE SST response are strongly driven by zonal advection (correlation of 0.92 and regression of 1.11 to the SST anomaly, Fig. 11a; Table 1). The atmospheric forcing terms variations are usually weaker (Fig. 11b), except when the WWE occurs close to the WPEE (stars on Fig. 11 indicate WWEs that occur within 20° of the WPEE). For these events, the amplitude of the air-sea fluxes driven cooling is much stronger (Fig. 11b), and contributes to limit the advective warming at the WPEE (Fig. 11a). The contributions of the atmospheric forcing and vertical processes to the WWE-induced maximum SST cooling are however weak (respectively 0.36 and -0.09 regression coefficients, Table 1), confirming the major role of horizontal advection in driving the diversity of the WWE SST response at the WPEE.

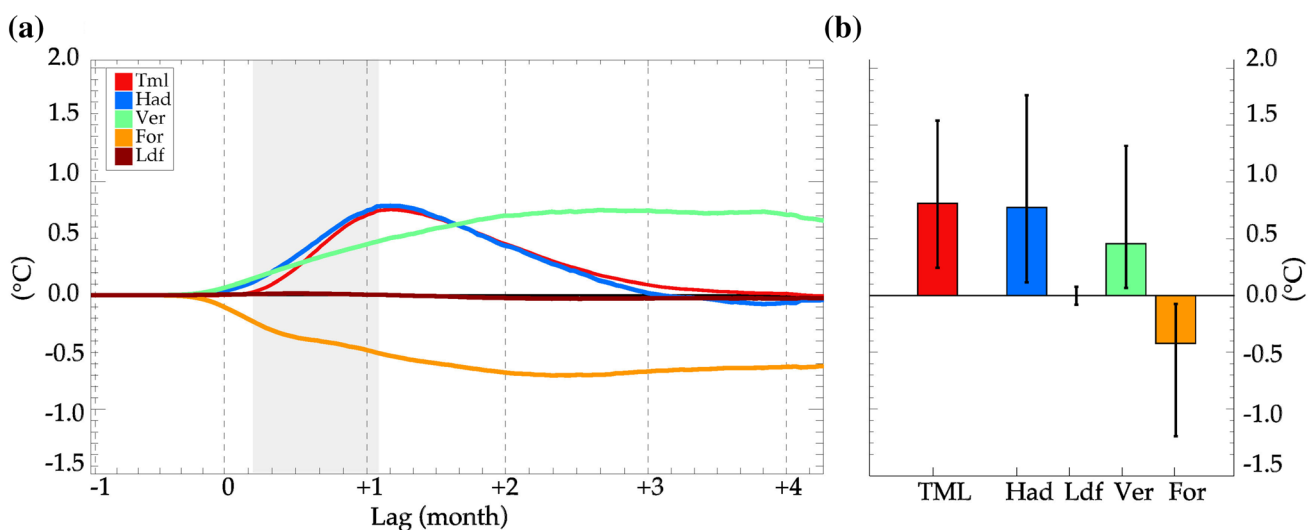


Fig. 10 Same as Fig. 7 but at the Warm Pool Eastern Edge (WPEE)

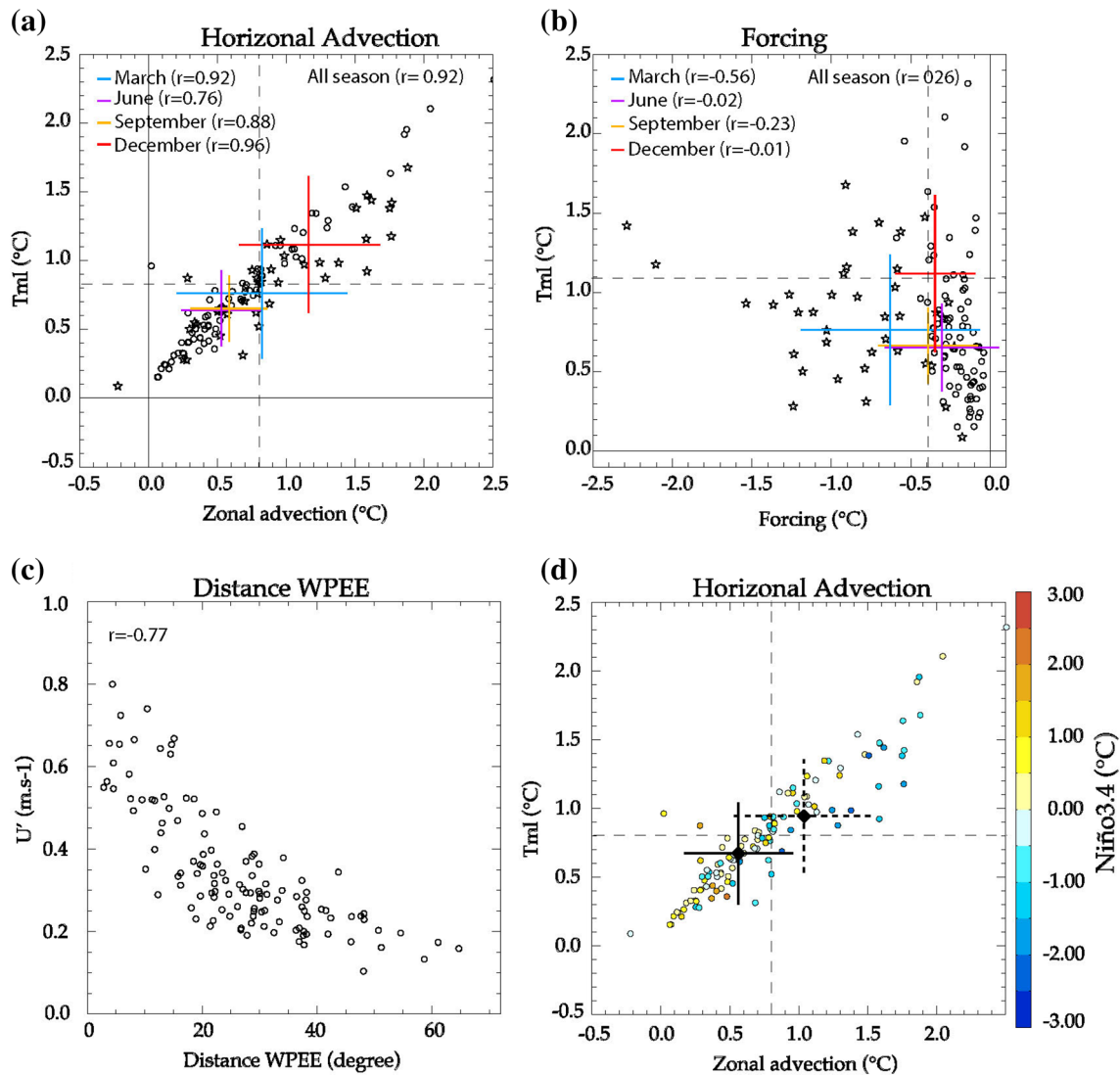


Fig. 11 **a, b** Same as Fig. 6 but at the WPEE. The *stars* indicate the WVEs that occur less than 20° away from the WPEE. **c** Scatterplot of the WVE-induced anomalous zonal current at the WPEE versus the distance between the WVE and WPEE. **d** Scatterplot of horizontal advection contribution against the WVE-induced SST response for each of the 120 WVEs. The *color* represents the values of the standardized average SST interannual anomalies in the Niño3.4

region during the WVE. The *black dots* and *crosses* show the mean and associated standard deviation for WVEs occurring during El Niño conditions (*full line*) and La Niña conditions (*dashed line*). We consider that a WVE occurs during El Niño (La Niña) conditions when the value of the ENSO index (computed as the standardized average interannual SST anomalies in Niño3.4 region) is above 0.5°C (below -0.5°C)

Owing to the dominant role of horizontal advection variations in driving the diversity in WVE SST response, we decompose this term as in Sect. 4.2. We also focus on zonal advection since the meridional advection only contributes weakly to the horizontal advection (regression coefficient of 0.84 of zonal advection onto horizontal advection). As in the western Pacific, the zonal advection is mainly driven by the advection of the background zonal SST gradient by the anomalous WVE-induced currents $-u'\partial_x\bar{T}$ (0.72 regression coefficient of $-u'\partial_x\bar{T}$ to $-(u\partial_x T)'$) with a weaker influence of $-u'\partial_x T'$ (0.22 regression

coefficient). The advection by anomalous currents $-u'\partial_x\bar{T}$ is correlated with both the WVE-induced current anomaly u' (0.71) and background SST gradient $\partial_x\bar{T}$ (-0.70), unlike in the western Pacific where only $\partial_x\bar{T}$ mattered. At a fixed location, the WVE response u' does not vary significantly as a function of the background oceanic state (Fig. 6e). The WPEE is however moving and its distance to the fixed-location WVEs in our experiments varies. Figure 11c shows that the amplitude of the WVE-induced current anomaly u' at the WPEE decays roughly

exponentially with the distance to the WPEE, with a typical inferred decay timescale of ~ 11 days (estimated as λ/c_1 where λ is the zonal decay scale and $c_1 = 2.8 \text{ m s}^{-1}$ the first baroclinic Kelvin wave phase speed). As a result of this double control of advection, the correlation between u' and the WWE-induced SST anomalies ($r = -0.59$) and the correlation between $\partial_x \bar{T}$ and the WWE-induced SST anomalies ($r = 0.41$) are rather weak. The control of the WWE-induced warming by a large-scale variable such as the mean zonal temperature gradient is thus weaker at the WPEE than in the western Pacific.

The amplitude of the WWE-induced warming varies seasonally (coloured crosses on Fig. 11a, b), being roughly twice as large for WWEs occurring in December (1.1°C) as during other seasons. This behaviour can directly be related to the larger zonal SST gradient in that season (not shown), consistent with the findings of Harrison and Schopf (1984). Although the seasonal control of the SST response diversity is slightly larger at the WPEE than in the western Pacific, interannual variations are still the dominant source of diversity for the zonal SST gradient (the interannual standard deviation of $0.3^\circ\text{C}/10^\circ$ longitude is about 70% larger than the seasonal standard deviation). Although interannual variability dominates the zonal SST gradient variability, it does not exhibit any significant relationship with ENSO (no significant lead or lag correlation with the main ENSO indices; not shown). On the other hand, the WPEE position, which controls the amplitude of the WWE-induced current anomaly u' at the WPEE, is largely influenced by ENSO ($r = 0.87$; not shown). However, while WWE-induced SST anomalies at the WPEE are somewhat larger during La Niñas than during El Niño

conditions (0.9°C against 0.6°C , respectively, see black crosses on Fig. 11d), there is a large spread in both cases and this difference is not statistically significant. As a result of the double control of advection, ENSO variations are not the primary source of WWE-induced SST response diversity at the WPEE. In addition, since the location of the WWE is not predictable at long leads, the u' anomaly at the WPEE is not predictable either.

In this section, we have shown that the idealised WWEs induce a 0.8°C average warming at the WPEE through zonal advection by the eastward current anomalies associated with the WWE-induced downwelling Kelvin wave. This advective warming can however vary by an order of magnitude mainly due to two effects. First, the intensity of the interannual SST zonal gradient at the WPEE can modulate the advective term. Second, the eastward current at the WPEE decays non-linearly with the distance between the WWE and the WPEE, itself also varying at interannual timescale. This results in a weaker warming if the WWE is far from the WPEE. The variations of the zonal SST gradient at the WPEE are also not strongly correlated with ENSO, resulting in a weaker ENSO control of the WWE-induced SST anomalies near the WPEE than in the western Pacific.

3.4 The eastern Pacific

This section finally addresses the mechanisms responsible for the warming downstream of the Kelvin wave path, in the eastern Pacific. Figure 12 shows that the SST warming starts 1 month after the WWE occurrence and reaches a 0.8°C maximum 3 months after the event. The growth

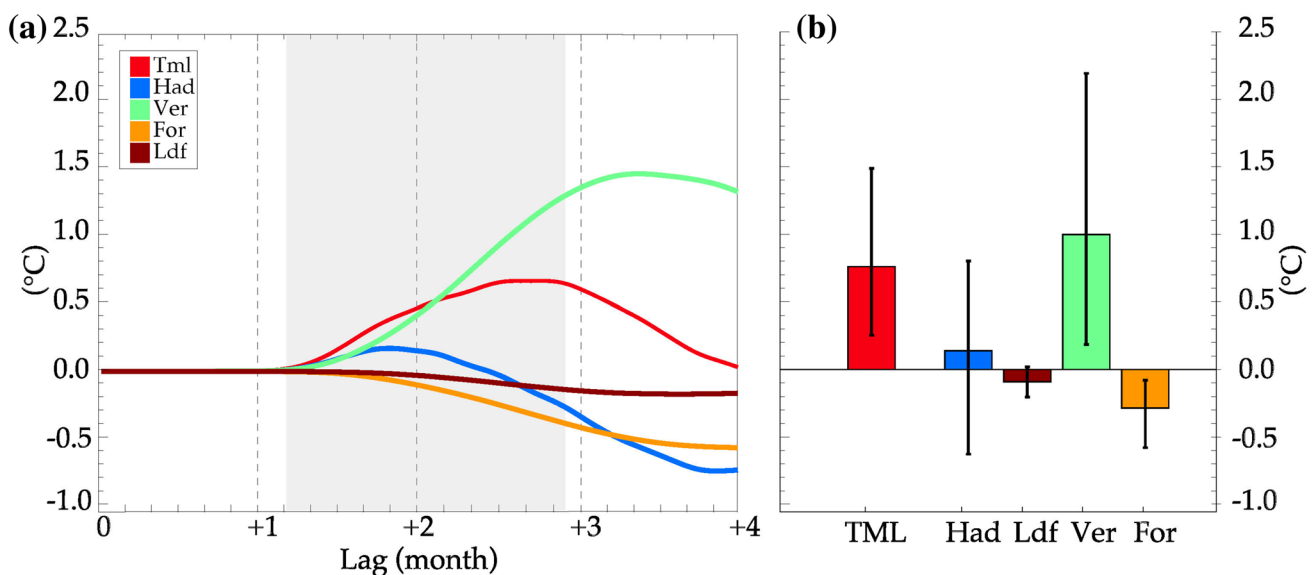


Fig. 12 Same as Fig. 5 but for the eastern Pacific region

of this positive SST anomaly is consistent with the vertical terms contribution evolution, while the contributions from horizontal and atmospheric forcing terms are relatively modest. The SST anomaly in the eastern Pacific is always positive for the 120 WWEs but its amplitude can vary by an order of magnitude as in the other regions, ranging from 0.2 to 1.5 °C (Fig. 12b). Vertical terms are largely responsible for the strong mean warming and also exhibit a strong variability, ranging from 0.2 to 2.3 °C. In the eastern Pacific, the negative contribution from the surface forcing term is due to the weak restoring to the model climatology used in our experimental setup and displays a weaker diversity (about one-third) than that of other terms. The horizontal advection term does not contribute to the mean warming but exhibits large variations, ranging from -0.6 to 0.6 °C (Fig. 12b). This significant role of horizontal advection on the intraseasonal SST budget in the eastern Pacific was noted in several studies (Lucas et al. 2010; Halkides and Lee 2011) and could be related both to anomalous advection of background SST gradient by Kelvin Wave-induced horizontal currents and to SST variability related to Tropical Instability Wave (TIW) activity in this region (e.g. Harrison and Giese 1988; Weidman et al. 1999; Vialard et al. 2001; Menkes et al. 2006).

Variations in the WWE SST response are strongly driven by vertical processes (correlation of 0.71 and regression of 1.23 to the SST anomaly, Fig. 13a; Table 1). Variations of the horizontal advection term are usually weaker (Fig. 13b) and do not strongly contribute to the amplitude of SST warming (correlation of 0.21 and regression coefficient of 0.21, Fig. 13b; Table 1), confirming the major role of vertical processes in driving the diversity of the WWE SST response in the eastern Pacific.

We now explore the control of vertical processes (upwelling, mixing and entrainment into the mixed layer) by large-scale oceanic properties. Both the thermocline position and the local wind stress are expected to influence the intensity of the vertical process changes in response to the WWE-driven thermocline depth anomalies. First, an anomalously shallow thermocline is associated with subsurface cold water close to the surface, which should favour larger vertical process variations in response to WWE-driven thermocline depth anomalies. Second, when the wind stress is strong, the mixed layer deepens close to the top thermocline, and WWE-driven variations of thermocline depth can thus have a large impact on the vertical term. In contrast, the mixed layer is more decoupled from the thermocline in calmer wind conditions, resulting in a lesser influence of WWE-driven thermocline deepening on the surface layer heat budget. This is verified in Fig. 14, which shows the vertical term variations as a function of both the local background thermocline depth and the wind stress. A

bilinear model is able to fit the vertical term with a 0.7 skill, with wind variations contributing more to WWE-induced vertical processes than thermocline depth variations ($VER = -0.36 D20^* + 0.49 TAUM^*$ where the star indicates unbiased variables normalized by their standard deviation). This appears in contrast to the interannual timescale, where SST anomalies are usually quite well related to thermocline depth anomalies in the eastern Pacific (e.g. Zelle et al. 2004), a point further discussed in Sect. 4.

While thermocline variations are largest interannually in the eastern box (standard deviation of 4.7 m/17.7 m for the seasonal/interannual components), wind stress variations are dominated by the seasonal cycle (standard deviation of 0.014/0.008 N m⁻²), with the strongest wind stress occurring in July–August, i.e., when the June WWE-induced sea level signals reaches the eastern Pacific. As a result, Fig. 13a reveals a significant seasonal modulation of the vertical mixing contribution to the WWE-induced warming in the eastern Pacific. WWEs occurring in June produce a stronger (2.2 °C on average) vertical mixing anomalies than during other seasons (~0.7 °C on average). This seasonal difference however does not cause a very large difference in terms of WWE SST response (only ~1.2 °C compared to ~0.7 °C on average during other seasons). This may be due to the strong TIW activity in August. TIWs tend to warm up the Equator, mainly through horizontal advection processes (Vialard et al. 2001). The deepening of the thermocline associated with the passage of a Kelvin wave reduces the TIW activity, and thus induces an anomalous cooling through horizontal advection (Fig. 13b), which limits the warm anomalies associated with vertical mixing, in agreement with Qiao and Weisberg (1995).

In contrast to the western Pacific, and as for the WPEE, the WWE-driven SST anomalies in the eastern Pacific are not affected by ENSO with either large or weak anomalies during both El Niño and La Niña conditions (Fig. 13c). This is probably because the background thermocline depth (which is clearly linked to ENSO with a 0.82 correlation with Niño3 SST index) is not the main parameter that controls WWE-induced SST response there. Indeed both local wind stress variations and the rectification due to Tropical Instability Waves are also key players.

In this section, we have shown that WWEs drive a mean eastern Pacific warming that reaches a maximum 3 months after the WWE. The amplitude of this SST change can vary by one order of magnitude depending on the background oceanic conditions, mainly through a modulation of the warming by vertical processes. The intensity of the WWE-driven vertical processes anomaly is primarily driven by seasonal wind stress variations and, to a lesser extent, by thermocline depth interannual anomalies. There is however no clear modulation of the

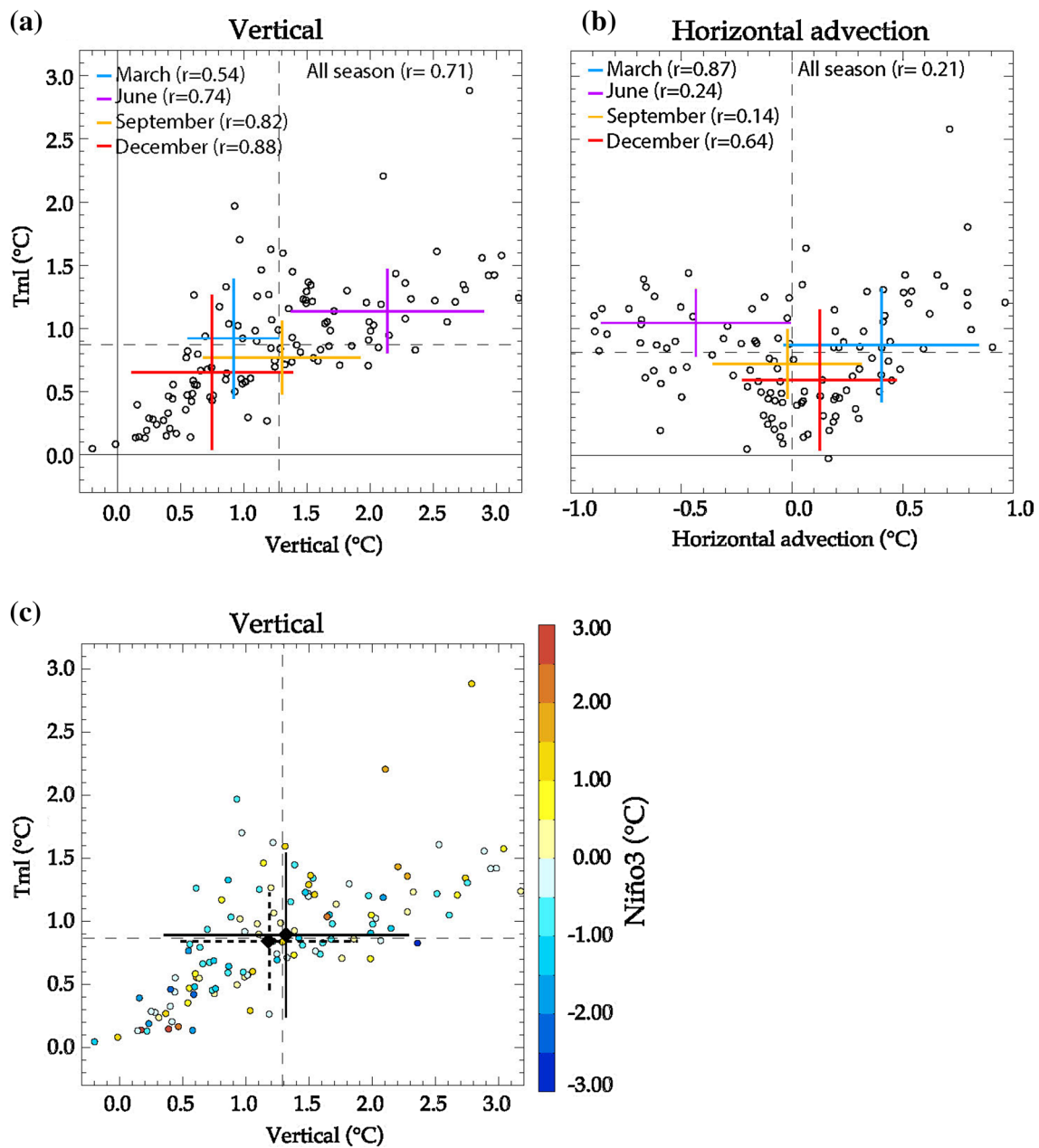


Fig. 13 Scatterplot of **a** vertical processes and **b** horizontal advection contribution against the SST response to the WVE, at the time of the peak SST anomaly in the eastern Pacific region for each of the 120 applied WVEs. The *dashed lines* indicate mean values. The *coloured crosses* indicate the mean values individually for each of the four different seasons, with the length of each arm of the cross indicating the standard deviation. The correlation between the paired variables are given on the *top left* of each panel both for the whole year and individual seasons. **c** Scatterplot of vertical processes contribution

against the WVE-induced SST response for each of the 120 WVEs. The *color* represents the values of the standardized average SST inter-annual anomalies in the Niño3.4 region during the occurrence of each WVE. The *black dots* and *crosses* show the mean and the associated standard deviation for the WVE occurring during El Niño conditions (*full line*) and La Niña conditions (*dashed line*). We consider that a WVE occurs during El Niño (La Niña) conditions when the value of the ENSO index (computed as the standardized average interannual SST anomalies in Niño3.4 region) is above 0.5 °C (below -0.5 °C)

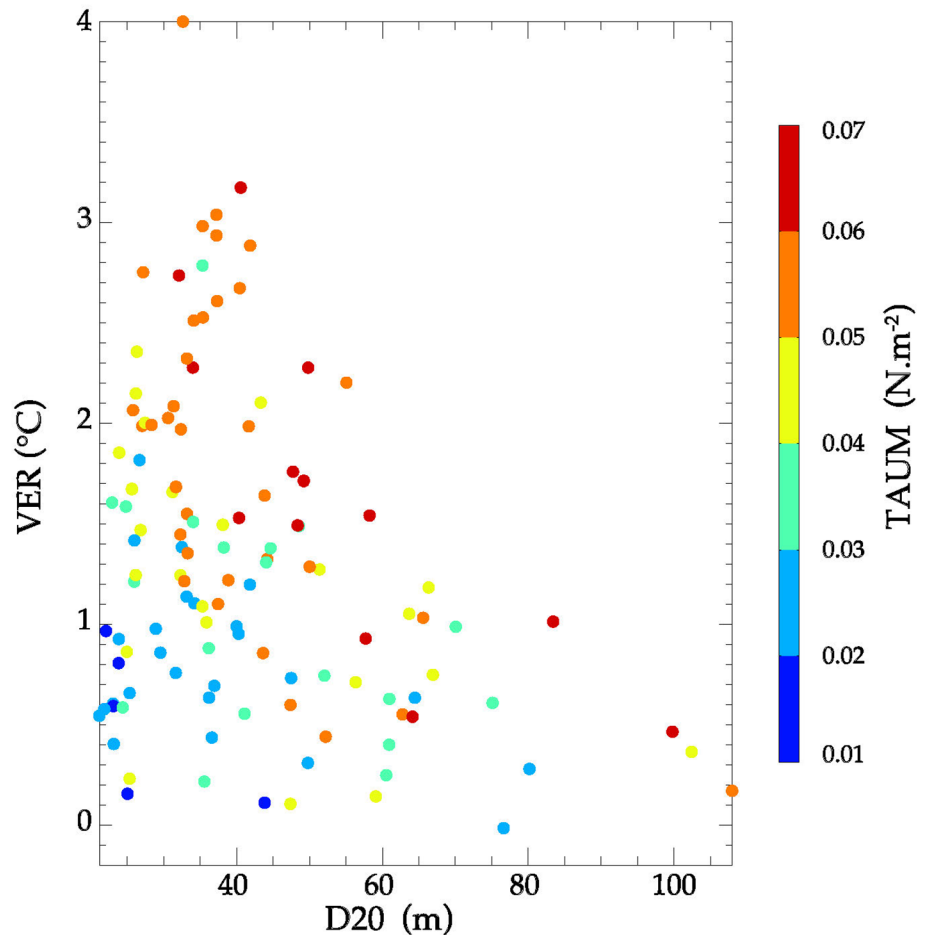
SST anomalies by pre-existing large-scale properties: the WVE-driven SST anomaly in the eastern box only has a 0.24 correlation with the ENSO driven thermocline depth anomalies in that region.

4 Summary and discussion

4.1 Summary

Westerly Wind Events (WVEs) play a key role in ENSO

Fig. 14 Scatterplot of vertical processes contribution (VER, °C) to the WWE-induced SST response at the time of the peak SST anomaly against the background thermocline depth (D20, m) in the reference simulation for each of the 120 WWEs. The color represents the background wind stress (TAUM, Nm^{-2}) in the reference simulation for each of the 120 WWEs. A bilinear fit of the time-integrated vertical term VER to D20^* and TAUM^* , where the star indicates unbiased variables (the average values have been removed), normalized by their standard deviation gives $\text{VER} = -0.36 \text{D20}^* + 0.49 \text{TAUM}^*$ and displays a 0.7 correlation skill



diversity and evolution. Their oceanic response is quite diverse in terms of magnitude, timing and location in both observational and modelling studies. Part of this diversity can be attributed to the WWE characteristics themselves, such as the intensity, duration and zonal fetch (Giese and Harrison 1990, 1991; Suzuki and Takeuchi 2000; Puy et al. 2016). The first result shown here is that the observed WWE dynamical oceanic response is more grounded by the WWE characteristics (correlation of 0.65 between the WEI and SLA, Fig. 3a) than the WWE SST response (correlation of 0.16 between the WEI and SSTA, Fig. 3b). Part of the diversity in the SST response to WWEs could be partly explained to the modulation by the background oceanic state. The present study investigates this source of WWE-induced SST response diversity using dedicated experiments with an ocean general circulation model, in which an identical idealised WWE is applied in 120 1-year long-simulations, every 3 months from 1980 to 2011.

In agreement with past literature (see Lengaigne et al. 2004a, b for a review and references therein), we show that the WWE SST response is characterized by a mean cooling under the WWE 15 days after the event, a warming at the WPEE at the passage of the downwelling Kelvin wave

and a warming in the eastern Pacific 2–3 months after the event. Our results however show that the amplitude of these WWE-induced SST signal can vary by one order of magnitude (typically between ~ 0.15 and 1.5°C) in these three regions and depend on the pre-existing oceanic background conditions.

In the western Pacific, a mixed layer temperature budget confirms the dominant role of WWE-related heat fluxes in driving the mean cooling under the WWEs in agreement with many previous studies that highlighted the major role played by heat fluxes in generating intraseasonal SST variations in this region (Anderson et al. 1996; Cronin and McPhaden 1997; Shinoda et al. 1998; Zhang and McPhaden 2000). However, horizontal advective processes are also shown to strongly modulate the amplitude of this cooling. This episodic role played by horizontal advection in driving the amplitude of the SST response to WWEs in the western Pacific was noted in other studies (e.g. Feng et al. 1998, 2000; Dourado and Caniaux 2001; Lengaigne et al. 2002). We find that this modulation by horizontal advection mainly operates through changes in the zonal SST gradient, as in Harrison and Schopf (1984). In contrast to their results, which emphasized the SST gradient

seasonal variations, we find a dominant role of its interannual variations: the cooling by mean atmospheric fluxes is strengthened during El Niños and weakened during La Niñas.

At the Eastern Edge of the Warm Pool (WPEE), the mean warming and its amplitude variations are both controlled by horizontal advection. The dominant role played by anomalous horizontal advection of the background SST field in driving the WWE-driven variations in the central Pacific is in line with previous work (Schopf and Harrison 1983; Harrison and Schopf 1984; Harrison and Craig 1993; Boulanger et al. 2001; Lengaigne et al. 2002). Our results show that the intensity of the WWE-induced cooling is more weakly modulated by the ENSO phase than that in the western Pacific for two reasons. First, the WPEE location is only weakly correlated with ENSO indices and, second, the intensity of the WWE-induced current anomalies, which are non-linearly related to the distance between the WWE and WPEE, also play a central role in modulating the advection.

Finally, the mean warming and its diversity in the eastern Pacific are largely controlled by vertical processes, which drive the WWEs SST response in this region (Zhang 2001; McPhaden 2002; Halkides and Lee 2011). Present results also show variations in the horizontal advection term, which has also been acknowledged as a potential contributor to the intraseasonal SST variability in this region (Lucas et al. 2010; Halkides and Lee 2011). We also show that the background wind stress and thermocline depth both control the intensity of the WWE-driven vertical processes. But due to the “noise” associated with Tropical Instability Waves and their rectification effect on the SST in the eastern Pacific, the WWE-induced SST anomaly is more difficult to relate to pre-existing large-scale properties there.

4.2 Discussion

In the western Pacific, we have shown that the mean WWE heat-flux anomaly-induced cooling can strongly be modulated by zonal advection. It must be noticed that we however neglected an important factor that is likely to strongly contribute to the diversity of the amplitude of this western Pacific cooling under WWEs in our experimental framework. As illustrated on Fig. 4 and discussed in Sect. 2.2, there is indeed a strong diversity in the surface heat flux anomalies associated with WWEs of similar magnitude: the heat flux anomaly reaches almost -200 W m^{-2} for the December 1996 WWE while it is much weaker for that of March 1997 ($\sim -50 \text{ W m}^{-2}$). This surface heat flux diversity will of course result in a strong diversity of the SST cooling under the WWE, which will combine with the modulation of the mean SST response by interannual changes in the zonal SST gradient.

In the eastern Pacific, we have shown that the WWE-driven effect of vertical processes on SST was driven both by background thermocline depth and local wind stress. This appears in contrast to the interannual timescale, where only thermocline variations modulate the depth of subsurface cold waters and hence the efficiency of the surface cooling through vertical mixing (e.g. Zelle et al. 2004). This previously documented relation explains why SST and the large thermocline depth interannual variations (-40 to 60 m) are well correlated in the eastern Pacific in observations (corr. 0.85, Fig. 15a). Figure 15b (corr. 0.86) shows the same analysis for the model, and displays a similar behaviour, confirming the model’s ability to produce the right physical balance at interannual timescales. This therefore suggests that the physics controlling the cooling by vertical processes are different at intraseasonal and interannual timescales. The role of local wind driven mixing (and horizontal advection) in driving a substantial part of the intraseasonal SST variations in the eastern Pacific shown here has also been noted by Halkides and Lee (2011). We hypothesize that this may be the result of the mixed layer depth and wind anomalies are in closer balance at interannual than at intraseasonal timescales, but the root cause for these different behaviours has yet to be fully understood.

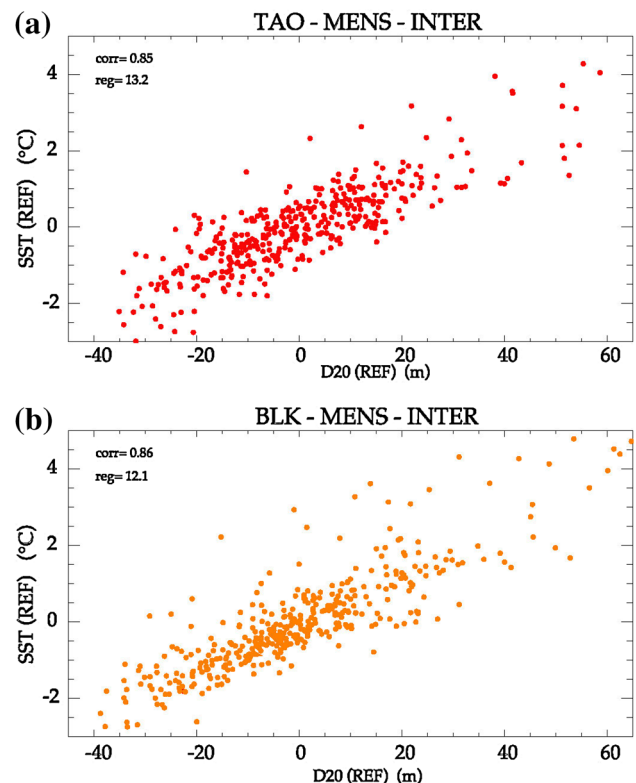


Fig. 15 Scatterplot of interannual SST anomalies versus interannual D20 anomalies in the eastern Pacific box, from **a** TAO observations and **b** the BLK simulation

Numerous studies explored the sensitivity of the Kelvin waves characteristics to the mean oceanic background conditions (Gill 1982; Busalacchi and Cane 1988; Giese and Harrison 1990; Benestad et al. 2002; Shinoda et al. 2008; Dewitte et al. 2008; Mosquera-Vasquez et al. 2014) but only a couple of studies have investigated the sensitivity of the SST response to the mean oceanic background conditions (Schopf and Harrison 1983; Harrison and Schopf 1984). Our findings generally agree with these seminal studies, and confirm the seasonal dependence of the amplitude of the WWE-induced SST warming at the WPEE. The dedicated idealised modelling strategy devised here has further shown that the interannual oceanic background variations are the dominant source of diversity for the WWE-induced SST changes.

The impact of ENSO variations on the WWE-driven SST anomalies and Kelvin waves characteristics is

summarized in Fig. 16, which provides time-longitude composites of the SST and thermocline depth response to WWEs occurring during El Niño and La Niña conditions, as well as their differences. In agreement with Fig. 8c, the western Pacific WWE-induced SST cooling is stronger during El Niño than during La Niña, with a maximum difference of about 1 °C. This cooling also occurs over a larger longitude range (50° against 30° during La Niña conditions). Indeed, as the warm pool is constrained further westward during cold conditions, the WWE-driven eastward zonal advection of warm water will more efficiently limit the cooling by WWE-driven heat fluxes during La Niña events (Fig. 16b).

Another significant difference between the WWE response during the two phases of ENSO consists of a stronger warming during El Niño conditions in the far eastern Pacific (Fig. 16c). This difference is consistent with the

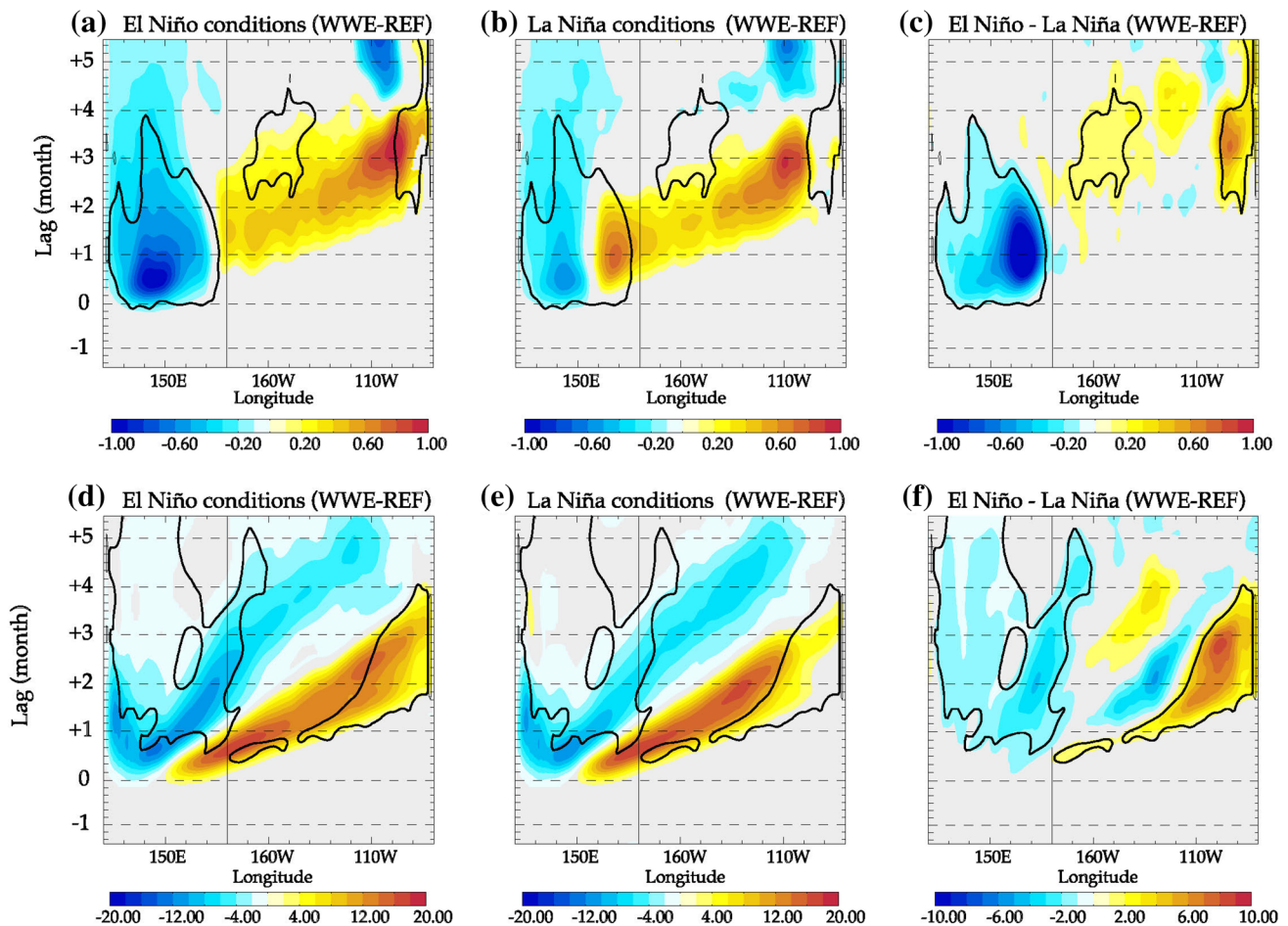


Fig. 16 (*1st row*) Time-longitude section of the 2°N–2°S average composite of the SST response to the WWEs during **a** El Niño conditions, **b** La Niña conditions and **c** the difference between **a** and **b**. (*2nd row*) Same for the D20 response. We consider that a WWE occur during El Niño (La Niña) conditions when the value of our ENSO index (computed as the standardized average interannual SST

anomalies in Niño3.4 region) is above 0.5 (below -0.5). Grey areas correspond to the composite values that are not significantly different from zero at the 95% confidence level. The black contour shows differences between El Niño and La Niña composites that are significantly different from zero at the 95% confidence level

most efficient eastward penetration of the downwelling Kelvin waves into the far eastern Pacific during El Niño conditions, (Benestad et al. 2002; Fig. 16d–f). While the Kelvin wave signal fades in the eastern Pacific during la Niña conditions (Fig. 16e), it reaches the coasts of South America during El Niño conditions (Fig. 16d). These results are also consistent with the findings of Dewitte et al. (2008) and Mosquera-Vasquez et al. (2014).

These results regarding the sensitivity of the WWE-induced response to the ENSO phase are more difficult to compare with Vecchi and Harrison (2000). Our modelling approach allows diagnosing the ocean response to WWEs as a difference between experiments with a WWE minus one without. This is obviously not possible in observations, for which Vecchi and Harrison (2000) compare SST changes in presence and absence of WWEs for different phases of El Niño. They find that WWEs occurring during regular conditions drive a significant warming over the central and eastern Pacific, while WWEs occurring during El Niño do not drive an equatorial warming but rather maintain the warm waters warm. In our anomalous framework, “maintaining warm water warm” results in a warm anomaly, relative to a run without WWEs where the SST cools. In addition, applying the same compositing methodology as in Vecchi and Harrison (2000) to our BLK simulation (their Fig. 4) indeed results in a very similar response to that described by Vecchi and Harrison (2000) (not shown). There is hence no contradiction between Vecchi and Harrison (2000) and our results, which are just presented in a different way (anomaly framework) in our study.

Our results demonstrate that the amplitude of the SST response to a WWE strongly depends on the pre-existing oceanic conditions, and exhibit a range of variations between 0 and 1.5 °C in all considered regions. The amplitude of the warming is however not clearly related to large-scale properties nor modulated by ENSO near the warm pool eastern edge, nor in the eastern Pacific. The amplitude of the cooling is better related to ENSO (more specifically to the Niño4 index) for the western Pacific cooling, but the diversity in the surface heat flux perturbations associated with WWE noted above may blur this relation. The practical implication for ENSO prediction is however not obvious, given the short prediction lead-time of WWEs. The modulation of the WWE SST response by the mean oceanic conditions near the WPEE may even act to limit predictability. Indeed this modulation depends both on the WWE position relative to the WPEE and on the zonal SST gradient at the WPEE, neither of them related to ENSO nor likely predictable at lead-times longer than a few weeks. The lack of clear improvement of ENSO prediction skill since the 2000s (Barnston and Tippett 2012) may hence tell us we could have reached limits of ENSO predictability as provided by large-scale precursors in the Pacific ocean.

Acknowledgements This work was supported by Agence Nationale de la Recherche (ANR) projects METRO, Grant No. 2010-BLAN-616-01, MORDICUS, Grant No. ANR-13-SENV-0002, and the Belmont project GOTHAM, Grant No. ANR-15-JCLI-0004-01, as well as the SPECS project funded by the European Commission’s Seventh Framework Research Programme under the Grant agreement 308378. We gratefully acknowledge Christophe Cassou, Marie-Pierre Moine, Laure Coquart and Stéphane Sénési for discussions and help with the model. Computations were carried out at the CNRS supercomputing centre (IDRIS). This work was done while Matthieu Lengaigne was a visiting scientist at the National Institute of Oceanography (Goa, India), thanks to Institut de Recherche pour le Développement (IRD) funding.

References

- Anderson SP, Weller RA, Lukas RB (1996) Surface buoyancy forcing and the mixed layer of the western Pacific warm pool : observations and 1d model results. *J Clim* 9(12):3056–3085
- Barnston A, Tippett M (2012) Skill of real-time seasonal ENSO model predictions during 2002–11: is our capability increasing? *Bull Am Meteorol Soc* 93(5):ES48–ES50
- Barsugli JJ, Sardeshmukh PD (2002) Global atmospheric sensitivity to tropical SST anomalies throughout the Indo-Pacific basin. *J Clim* 15(23):3427–3442
- Belamari S, Redelsperger J-L, Pontaud M (2003) Dynamic role of a westerly wind burst in triggering an equatorial Pacific warm event. *J Clim* 16(12):1869–1890
- Benestad RE, Sutton RT, Anderson DL (2002) The effect of El Niño on intraseasonal Kelvin waves. *Q J R Meteorol Soc* 128(582):1277–1291
- Bjerknes J (1966) A possible response of the atmospheric Hadley circulation to equatorial anomalies of ocean temperature. *Tellus* 18(4):820–829
- Blanke B, Delecluse P (1993) Variability of the tropical Atlantic ocean simulated by a general circulation model with two different mixed-layer physics. *J Phys Oceanogr* 23(7):1363–1388
- Boulangier J-P, Menkes C (1999) Long equatorial wave reflection in the Pacific Ocean from TOPEX/POSEIDON data during the 1992–1998 period. *Clim Dyn* 15(3):205–225
- Boulangier J-P, Durand E, Duvel JP, Menkes C, Delecluse P, Imbard M, Lengaigne M, Madec G, Masson S (2001) Role of non-linear oceanic processes in the response to westerly wind events: new implications for the 1997 El Niño onset. *Geophys Res Lett* 28(8):1603–1606
- Boulangier J-P, Menkes C, Lengaigne M (2004) Role of high- and low-frequency winds and wave reflection in the onset, growth and termination of the 1997–1998 El Niño. *Clim Dyn* 22(2–3):267–280
- Busalacchi AJ, Cane MA (1988) The effect of varying stratification on low-frequency equatorial motions. *J Phys Oceanogr* 18(6):801–812
- Capotondi A, Wittenberg AT, Newman M, Di Lorenzo E, Yu JY, Brannon P, Jin FF (2015) Understanding ENSO diversity. *Bull Am Meteorol Soc* 96(6):921–938
- Chen D, Lian T, Fu C, Cane MA, Tang Y, Murtugudde R (2015). Strong influence of westerly wind bursts on El Niño diversity. *Nat Publ Group* 8(5):339–345
- Chiodi A, Harrison DE, Vecchi A (2014) Subseasonal atmospheric variability and El Niño Waveguide warming: observed effects of the Madden-Julian oscillation and westerly wind events. *J Clim* 27(10):3619–3642
- Cronin MF, McPhaden MJ (1997) The upper ocean heat balance in the western equatorial warm pool during September–December 1992. *J Geophys Res* 102(C4):8533–8553

- Cronin MF, McPhaden MJ (1998) Upper ocean salinity balance in the western equatorial Pacific. *J Geophys Res Oceans* 103(C12):27567–27587
- Dee D, Uppala S, Simmons A, Berrisford P, Poli P, Kobayashi S, Andrae U, Balma-seda M, Balsamo G, Bauer P et al (2011) The era-interim reanalysis: configuration and performance of the data assimilation system. *Q J R Meteorol Soc* 137(656):553–597
- Delcroix T, Eldin G, McPhaden M, Morlière A (1993) Effects of westerly wind bursts upon the western equatorial pacific ocean, February–April 1991. *J Geophys Res Oceans* 98(C9):16379–16385
- Dewitte B, Purca S, Illig S, Renault L, Giese BS (2008) Low-frequency modulation of intraseasonal equatorial kelvin wave activity in the pacific from soda: 1958–2001. *J Clim* 21(22):6060–6069
- Dourado M, Caniaux G (2001) Surface heat budget in an oceanic simulation using data from tropical ocean-global atmosphere coupled ocean–atmosphere response experiment. *J Geophys Res* 108:16
- Drushka K, Bellenger H, Guilyardi E, Lengaigne M, Vialard J, Madec G (2015) Processes driving intraseasonal displacements of the eastern edge of the warm pool: the contribution of westerly wind events. *Clim Dyn* 44(3–4):735–755
- Dussin R, Barnier B (2013) The making of dfs 5.1. Drakkar Project Rep
- Eisenman I, Yu L, Tziperman E (2005) Westerly wind bursts: ENSO's tail rather than the dog? *J Clim* 18(24):5224–5238
- Fairall C, Bradley E, Rogers D, Edson J, Youngs G (1996) Bulk parameterization of air-sea fluxes for tropical ocean-global atmosphere coupled-ocean atmosphere response. *Geophys Res* 101:3747–3764
- Fedorov AV (2002) The response of the coupled tropical ocean–atmosphere to westerly wind bursts. *Q J R Meteorol Soc* 128(579):1–23
- Fedorov AV, Hu S, Lengaigne M, Guilyardi E (2014) The impact of westerly wind bursts and ocean initial state on the development, and diversity of el niño events. *Clim Dyn* 44(5–6):1381–1401
- Feng M, Hacker P, Lukas R (1998) Upper ocean heat and salt balances in response to a westerly wind burst in the western equatorial pacific during toga coare. *J Geophys Res* 103(10):289–310
- Feng M, Lukas R, Hacker P, Weller RA, Anderson SP (2000) Upper-ocean heat and salt balances in the western equatorial pacific in response to the intraseasonal oscillation during toga coare. *J Clim* 13(14):2409–2427
- Gebbie G, Eisenman I, Wittenberg AT, Tziperman E (2007) Modulation of westerly wind bursts by sea surface temperature: a semistochastic feedback for ENSO. *J Atmos Sci* 64(9):3281–3295
- Giese BS, Harrison DE (1990) Aspects of the Kelvin wave response to episodic wind forcing. *J Geophys Res Oceans* 95(C5):7289–7312
- Giese BS, Harrison D (1991) Eastern equatorial pacific response to three composite westerly wind types. *J Geophys Res Oceans* (1978–2012) 96(S01):3239–3248
- Gill AE (1982) *Atmosphere–ocean dynamics*, volume 30. Academic Press, New Jersey
- Graham N, Barnett T (1987) Sea surface temperature, surface wind divergence, and convection over tropical oceans. *Science* 238(4827):657–659
- Guilyardi E, Madec G, Terray L (2001) The role of lateral ocean physics in the upper ocean thermal balance of a coupled ocean–atmosphere gcm. *Clim Dyn* 17(8):589–599
- Guilyardi E, Cai W, Collins M, Fedorov AV, Jin F-F, Kumar A, Sun D-Z, Wittenberg A (2012) New strategies for evaluating ENSO processes in climate models. *Bull Am Meteorol Soc* 93(2):235
- Halkides D, Lee T (2011) Mechanisms controlling seasonal mixed layer temperature and salinity in the southwestern tropical indian ocean. *Dyn Atmos Oceans* 51(3):77–93
- Harrison D, Craig A (1993) Ocean model studies of upper-ocean variability at 0°, 160° w during the 1982–1983 enso: local and remotely forced response. *J Phys Oceanogr* 23(3):425–451
- Harrison D, Giese BS (1988) Remote westerly wind forcing of the eastern equatorial pacific; some model results. *Geophys Res Lett* 15(8):804–807
- Harrison DE, Schopf PS (1984) Kelvin-wave-induced anomalous advection and the onset of surface warming in El Niño events. *Mon Weather Rev* 112(5):923–933
- Hewitt HT, Copsey D, Culverwell ID, Harris CM, Hill RSR, Keen AB, McLaren AJ, Hunke EC (2011) Design and implementation of the infrastructure of HadGEM3: the next-generation Met Office climate modelling system. *Geosci Model Dev* 4(2):223–253
- Hu S, Fedorov AV, Lengaigne M, Guilyardi E (2014) The impact of westerly wind bursts on the diversity and predictability of El Niño events: an ocean energetics perspective. *Geophys Res Lett* 41:4654–4663
- Jackett DR, Mcdougall TJ (1995) Minimal adjustment of hydrographic profiles to achieve static stability. *J Atmos Oceanic Technol* 12(2):381–389
- Jin F-F (1997) An equatorial ocean recharge paradigm for ENSO. Part I: conceptual model. *J Atmos Sci* 54(7):811–829
- Jin F-F, Lin L, Timmermann A, Zhao J (2007) Ensemble-mean dynamics of the ENSO recharge oscillator under state-dependent stochastic forcing. *Geophys Res Lett* 34(3):L03807
- Kindle JC, Phoebus PA (1995) The ocean response to operational westerly wind bursts during the 1991–1992 el nino. *J Geophys Res Oceans* (1978–2012) 100(C3):4893–4920
- Kleeman R, Moore AM (1999) A new method for determining the reliability of dynamical enso predictions. *Mon Weather Rev* 127(5):694–705
- Kumar BP, Vialard J, Lengaigne M, Murty V, McPhaden M (2012) Tropflux: air-sea fluxes for the global tropical oceans—description and evaluation. *Clim Dyn* 38(7–8):1521–1543
- Kumar BP, Vialard J, Lengaigne M, Murty V, McPhaden M, Cronin M, Pinsard F, Reddy KG (2013) Tropflux wind stresses over the tropical oceans: evaluation and comparison with other products. *Clim Dyn* 40(7–8):2049–2071
- Lengaigne M, Boulanger J-P, Menkes C, Masson S, Madec G, Delecluse P (2002) Ocean response to the March 1997 westerly wind event. *J Geophys Res* 107(C12):8015
- Lengaigne M, Boulanger J-P, Menkes C, Madec G, Delecluse P, Guilyardi E, Slingo JM (2003a) The March 1997 westerly wind event and the onset of the 1997/98 El Niño: understanding the role of the atmospheric response. *J Clim* 16(20):3330–3343
- Lengaigne M, Madec G, Menkes C, Alory G (2003b) Impact of isopycnal mixing on the tropical ocean circulation. *J Geophys Res* 108(C11):3345. doi:10.1029/2002JC001704
- Lengaigne M, Boulanger J-P, Menkes C, Delecluse P, Slingo J (2004a) Westerly wind events in the Tropical Pacific and their influence on the coupled ocean–atmosphere system: a review. In: Wang C, Xie SP, Carton JA (eds) *Earth's climate*. American Geophysical Union, Washington, DC. doi:10.1029/147GM03
- Lengaigne M, Guilyardi E, Boulanger J-P, Menkes C, Delecluse P, Inness P, Cole J, Slingo JM (2004b) Triggering of El Niño by westerly wind events in a coupled general circulation model. *Clim Dyn* 23(6):601–620
- Lengaigne M, Menkes C, Aumont O, Gorgues T, Bopp L, André J-M, Madec G (2007) Influence of the oceanic biology on the tropical pacific climate in a coupled general circulation model. *Clim Dyn* 28(5):503–516
- Lian T, Chen D, Tang Y, Wu Q (2014) Effects of westerly wind bursts on El Niño: a new perspective. *Geophys Res Lett* 41:3522–3527. doi:10.1002/2014GL059989

- Lucas LE, Waliser DE, Murtugudde R (2010) Mechanisms governing sea surface temperature anomalies in the eastern tropical Pacific Ocean associated with the boreal winter Madden-Julian Oscillation. *J Geophys Res* 115:C05012. doi:[10.1029/2009JC005450](https://doi.org/10.1029/2009JC005450)
- Luther D, Harrison D (1984) Observing long-period fluctuations of surface winds in the tropical Pacific: Initial results from island data. *Mon Weather Rev* 112(2):285–302
- McPhaden MJ (1999) Genesis and evolution of the 1997–98 El Niño. *Science* 283(5404):950–954
- McPhaden MJ (2002) Mixed layer temperature balance on intraseasonal timescales in the equatorial Pacific Ocean. *J Clim* 15:2632–2647
- McPhaden MJ (2015) Playing hide and seek with El Niño. *Nat Clim Change* 5:791–795. doi:[10.1038/nclimate2775](https://doi.org/10.1038/nclimate2775)
- McPhaden MJ, Taft BA (1988) Dynamics of seasonal and intraseasonal variability in the eastern equatorial Pacific. *J Phys Oceanogr* 18(11):1713–1732
- McPhaden MJ, Bahr F, Du Penhoat Y, Firing E, Hayes SP, Niiler PP, Richardson PL, Toole JM (1992) The response of the western equatorial Pacific ocean to westerly wind bursts during November 1989 to January 1990. *J Geophys Res Oceans* 97(C9):14289–14303
- McPhaden MJ, Zhang X, Hendon HH, Wheeler MC (2006) Large scale dynamics and MJO forcing of ENSO variability. *Geophys Res Lett* 33(16):L16702
- Meinen CS, McPhaden MJ (2000) Observations of warm water volume changes in the equatorial Pacific and their relationship to El Niño and La Niña. *J Clim* 13(20):3551–3559
- Menkes CE, Vialard JG, Kennan SC, Boulanger J-P, Madec GV (2006) A modeling study of the impact of tropical instability waves on the heat budget of the eastern equatorial Pacific. *J Phys Oceanogr* 36(5):847–865
- Menkes C, Lengaigne M, Vialard J, Puy M, Marchesiello P, Cravatte S, Cambon G (2014). About the role of Westerly Wind Events in the possible development of an El Niño in 2014. *Geophys Res Lett*
- Mosquera-Vásquez K, Dewitte B, Illig S (2014) The central Pacific El Niño intraseasonal Kelvin wave. *J Geophys Res Oceans* 119(10):6605–6621
- Palmer TN, Mansfield DA (1984) Response of two atmospheric general circulation models to sea surface temperature anomalies in the tropical East and West Pacific. *Nature* 310:483–485
- Paulson CA, Simpson JJ (1977) Irradiance measurements in the upper ocean. *J Phys Oceanogr* 7(6):952–956
- Picaut J, Ioualalen M, Delcroix T, Masia F, Murtugudde R, Vialard J (2001) The oceanic zone of convergence on the eastern edge of the Pacific warm pool: a synthesis of results and implications for El Niño–Southern Oscillation and biogeochemical phenomena. *J Geophys Res Oceans* 106(C2):2363–2386
- Picaut J, Hackert E, Busalacchi AJ, Murtugudde R, Lagerloef GS (2002) Mechanisms of the 1997–1998 El Niño–La Niña, as inferred from space-based observations. *J Geophys Res Oceans* (1978–2012) 107(C5), 1–5
- Puy M, Vialard J, Lengaigne M, Guilyardi E (2016) Modulation of equatorial Pacific westerly/easterly wind events by the Madden-Julian oscillation and convectively-coupled Rossby waves. *Clim Dyn* 46:2155. doi:[10.1007/s00382-015-2695-x](https://doi.org/10.1007/s00382-015-2695-x)
- Qiao L, Weisberg RH (1995) Tropical instability wave kinematics: observations from the tropical instability wave experiment. *J Geophys Res Oceans* (1978–2012) 100(C5):8677–8693
- Richardson RA, Ginis I, Rothstein LM (1999) A numerical investigation of the local ocean response to westerly wind burst forcing in the western equatorial Pacific. *J Phys Oceanogr* 29(6):1334–1352
- Roulet G, Madec G (2000) Salt conservation, free surface, and varying levels: a new formulation for ocean general circulation models. *J Geophys Res Oceans* (1978–2012) 105(C10):23927–23942
- Schopf PS, Harrison DE (1983) On equatorial waves and El Niño. I. Influence of initial states on wave-induced currents and warming. *J Phys Oceanogr* 13(6):936–948
- Schopf PS, Suarez MJ (1988) Vacillations in a coupled ocean–atmosphere model. *J Atmos Sci* 45(3):549–566
- Shi L, Alves O, Hendon H (2009) The role of stochastic forcing in ensemble forecasts of the 1997/98 El Niño. *J Clim* 22(10):2526–2540
- Shinoda T, Hendon HH, Glick J (1998) Intraseasonal variability of surface fluxes and sea surface temperature in the tropical western Pacific and Indian oceans. *J Clim* 11(7):1685–1702
- Shinoda T, Roundy PE, Kiladis GN (2008) Variability of intraseasonal Kelvin waves in the equatorial Pacific ocean. *J Phys Oceanogr* 38(5):921–944
- Smyth WD, Hebert D, Moum JN (1996) Local ocean response to a multiphase westerly wind burst: 2. Thermal and freshwater responses. *J Geophys Res* 101(C10):22513
- Suzuki T, Takeuchi K (2000) Response of equatorial Pacific mean temperature field to intraseasonal wind forcing. *J Oceanogr* 56(5):485–494
- Trenberth KE, Branstator GW, Karoly D, Kumar A, Lau KM, Ropelewski C (1998) Progress during TOGA in understanding and modeling global teleconnections associated with tropical sea surface temperatures. *J Geophys Res* 103(C7):14291
- Uppala SM, Kållberg P, Simmons A, Andrae U, Bechtold V, Fiorino M, Gibson J, Haseler J, Hernandez A, Kelly G et al (2005) The era-40 re-analysis. *Q J R Meteorol Soc* 131(612):2961–3012
- Vecchi G, Harrison D (2000) Tropical Pacific sea surface temperature anomalies, El Niño, and equatorial westerly wind events. *J Clim* 13(11):1814–1830
- Vecchi G, Wittenberg AT (2010) El Niño and our future climate: where do we stand? *Wiley Interdisciplinary Reviews. Clim Change* 1(2):260–270
- Vecchi G, Wittenberg AT, Rosati A (2006) Reassessing the role of stochastic forcing in the 1997–1998 El Niño. *Geophys Res Lett* 33(1):L01706
- Vialard J, Menkes C, Boulanger J-P, Delecluse P, Guilyardi E, McPhaden MJ, Madec G (2001) A model study of oceanic mechanisms affecting equatorial Pacific sea surface temperature during the 1997–98 El Niño. *J Phys Oceanogr* 31(7):1649–1675
- Wang W, Chen M, Kumar A, Xue Y (2011) How important is intraseasonal surface wind variability to real-time ENSO prediction? *Geophys Res Lett* 38:L13705. doi:[10.1029/2011GL047684](https://doi.org/10.1029/2011GL047684)
- Weidman P, Mickler DL, Dayyani B, Born G (1999) Analysis of Legeckis eddies in the near-equatorial Pacific. *J Geophys Res Oceans* (1978–2012) 104(C4):7865–7887
- Zavala-Garay J, Zhang C, Moore AM, Kleeman R (2005) The linear response of ENSO to the Madden-Julian oscillation. *J Clim* 18(13):2441–2459
- Zelle H, Appeldoorn G, Burgers G, van Oldenborgh GJ (2004) The relationship between sea surface temperature and thermocline depth in the eastern equatorial Pacific. *J Phys Oceanogr* 34(3):643–655
- Zhang C (2001) Intraseasonal perturbations in sea surface temperatures of the equatorial eastern Pacific and their association with the Madden-Julian oscillation. *J Clim* 14(6):1309–1322
- Zhang C, McPhaden MJ (2000) Intraseasonal surface cooling in the equatorial western Pacific. *J Clim* 13(13):2261–2276
- Zhang KQ, Rothstein LM (1998) Modelling the oceanic response to westerly wind bursts in the western equatorial Pacific. *J Phys Oceanogr* 28(11):2227–2249